A Fluid-Mixture Type Algorithm for Compressible Multicomponent Flow with Mie–Grüneisen Equation of State

Keh-Ming Shyue

Department of Mathematics, National Taiwan University, Taipei, Taiwan 106, Republic of China
E-mail: shyue@math.ntu.edu.tw

A simple interface-capturing approach proposed previously by the author for efficient numerical resolution of multicomponent problems with a van der Waals fluid [*J. Comput. Phys.*, 156 (1999), pp. 43–88] is extended to a more general case with real materials characterized by a Mie–Grüneisen equation of state. As before, the flow regime of interests is assumed to be homogeneous with no jumps in the pressure and velocity (the normal component of it) across the interfaces that separate two regions of different fluid components. The algorithm uses a mixture type of the model system that is formed by combining the Euler equations of gas dynamics for the basic conserved variables and an additional set of effective equations for the problem-dependent material quantities. In this approach, the latter equations are introduced in the algorithm primarily for an easy computation of the pressure from the equation of state, and are derived so as to ensure a consistent modeling of the energy equation near the interfaces where two or more fluid components are present in a grid cell, and also the fulfillment of the mass equation in the other single component regions. A standard high-resolution wave propagation method designed originally for single component flows is generalized to solve the proposed system for multicomponent flows, giving an efficient implementation of the algorithm. Several numerical results are presented in both one and two space dimensions that show the feasibility of the method with the Roe Riemann solver as applied to a reasonable class of practical problems without introducing any spurious oscillations in the pressure near the interfaces. This includes results obtained using a multicomponent version of the AMRCLAW software package of Berger and LeVeque for the simulation of the impact of an underwater aluminum plate to a copper plate in two space dimensions. © 2001 Academic Press

Key Words: Godunov-type scheme; impact problems; Mie–Grüneisen equation of state; multicomponent flows; Roe approximate Riemann solver.

1. INTRODUCTION

In this paper, we describe extensions of a fluid-mixture type algorithm proposed previously by the author for efficient numerical resolution of multicomponent problems with a van der Waals gas (cf. [45]) to a more general case with materials characterized by a Mie–Grüneisen equation of state of the form

$$p(\rho, e) = p_{\text{ref}}(\rho) + \Gamma(\rho)\rho\,[e - e_{\text{ref}}(\rho)]. \tag{1}$$

Here p, ρ, and e denote the pressure, density, and specific internal energy of the flow, respectively; $\Gamma = (1/\rho)(\partial p/\partial e)|_\rho$ is the Grüneisen coefficient, and p_{ref}, e_{ref} are the properly chosen states of the pressure and internal energy along some reference curve (e.g., along an isentrope, a single shock Hugoniot, or the other empirically fitting curves) in order to match the experimental data of the material being examined. Note that, for simplicity, each of the expressions Γ, p_{ref}, and e_{ref} is taken as a function of the density only. Even with this simplification, the analytical form of the equation of state (1) is an adequate approximation to a wide variety of materials of interest. This includes some gaseous or solid explosives and solid metals under high pressure; see Section 2 for the details.

It is known that for a general multicomponent flow system (compressible or not), depending specifically on conditions such as the topological structure of the interfaces and jumps of fluid properties across them, one can distinguish various type of flow regimes of practical importance, e.g., annular flow, slug flow, bubbly flow, and so on (cf. [10, 49, 51, 53]). Among them, in this work (cf. [44, 45, 46] also), we are interested in problems arising from a so-called homogeneous flow in which there is typically a strong coupling between the motion of each fluid component, and assumes a simple flow condition with no jumps in the pressure and velocity (the normal component of it) across interfaces that separate two different fluid components. Consider a one-dimensional inviscid compressible flow, for example. The basic conservation laws for the fluid mixtures of mass, momentum, and energy are

$$\frac{\partial \rho}{\partial t} + \frac{\partial}{\partial x}(\rho u) = 0,$$

$$\frac{\partial}{\partial t}(\rho u) + \frac{\partial}{\partial x}(\rho u^2 + p) = 0, \tag{2}$$

$$\frac{\partial}{\partial t}(\rho E) + \frac{\partial}{\partial x}(\rho E u + p u) = 0,$$

respectively, where u is the particle velocity, and $E = e + u^2/2$ is the specific total energy. Clearly, (2) takes the same form as the standard Euler equations of gas dynamics for a single component flow, and has been used quite extensively in modeling the behavior of a homogeneous flow (cf. [44, 45, 46]). Note that, in contrast to the case mentioned above, the use of a separate set of equations for each fluid component is often preferred for nonhomogeneous multicomponent problems; see [2, 12, 39] for an example.

To solve a compressible multicomponent problem with a general. Mie–Grüneisen equation of state (1), we want to use an Eulerian formulation of the equations as in the form described in (2), and to employ a state-of-the-art shock capturing method on a uniform rectangular grid for numerical approximation. Aside from the basic properties that a numerical method should follow in regions where the solutions contain only a single component

(cf. [7]), one major problem in the method development of a multicomponent solver is the need to devise a proper model and treatment of the numerical mixing between more than one fluid component within a grid cell. For the homogeneous flow problems considered here, in particular, it is imperative to construct the method so that both the pressure and velocity remain in equilibrium without introducing any spurious oscillations for these mixture cells. With applications to materials modeled by (1), some representative methods of the previous efforts in this direction are the volume-of-fluid approach of Miller and Puckett [31], the two-phase flow approach of Saurel and Abgrall [41], and the ghost-fluid approach of Fedkiw *et al.* [13]; see also [47] for an Lagrangian–Eulerian approach and [18, 42] for other up-to-date multicomponent algorithms.

With (1), our approach to model grid cells that contain more than one fluid component follows essentially the same idea as developed in [44, 45] for stiffened and van der Waals gases, and is a further generalization of the quasi-conservative method of Abgrall [1] for ideal gases. That is to say, we begin by considering an interface-only problem in one dimension where both the pressure and velocity are constants in the domain, while there are jumps in the other material-dependent variables across some interfaces. Then, from the energy equation, we derive a set of effective equations for the mixtures of the problem-dependent material quantities near the interfaces, see (11a) and (11b), so as to ensure the pressure remains in equilibrium for this problem. As in the previous work [45], in order to keep the material quantities unchanged as it should be in a single component region for a more general problem with shock and rarefaction waves as well, we proceed to modify these equations and obtain (11c) and (11d).

Note that here because of the strongly nonlinear coupling between many of the material quantities in the Mie–Grüneisen equation of state (1), see Section 2, it is not possible to manipulate those equations further to find out a suitable effective equation for each of the material quantities as we have hope for in the van der Waals gas case [45], which yields the calculation of some of the material quantities from the equation of state an explicit step out of the question. To remedy this situation, through a process of splitting from the equation for the internal energy, we come up with a set of three equations, i.e., Eqs. (11c), (11e), and (11f), which together with a local model based on the volume fraction of fluid components within a grid cell can be used to the determination of the material-dependent functions Γ, p_{ref}, and e_{ref}. Therefore, we are able to compute the pressure from the equation of state in an easy manner with a reasonable amount of cost. A combination of the Euler's equation (2) with this set of three equations and the evolution equations for volume fractions gives a complete model system that is a viable one to use in our algorithm for numerical approximation of multicomponent problems. This will be discussed further in Section 3 for the one-dimensional case, and Section 6 for the multidimensional extension.

It should be mentioned that the multicomponent model we have derived, i.e., Eq. (12) or (23), is not written in the full conservation form, but is rather a quasi-conservative system of equations. Nevertheless, as in the case for single component flows, this model is a hyperbolic system when each physically relevant value of the state variables of the flow is defined in the region of thermodynamic stability; see Sections 2 and 3. As before (cf. [44, 45]), here we use the high-resolution method based on the wave-propagation viewpoint to compute approximate solution of the problem, giving an efficient implementation of the algorithm and also very accurate results for a variety of one- and two-dimensional problems; see Sections 5 and 6.1 for the details.

This paper is organized as follows. In Section 2, we discuss two important types of the curves (i.e., the isentropic and Hugoniot loci) for the reference states in the Mie–Grüneisen equation of state, and give some examples of interests for an explicit expression of the material-dependent functions Γ, p_{ref}, and e_{ref}. In Section 3, we describe in detail the construction of our fluid-mixture type multicomponent model in one dimension. The numerical method used to find approximate solution of the model system is briefly reviewed in Section 4. This includes some discussion of the approximate Riemann solver of Roe. One-dimensional results obtained using our multicomponent algorithm are shown in Section 5. In Section 6, we extend the one-dimensional algorithm to multiple space dimensions, and show some numerical results in two dimensions.

2. EQUATIONS OF STATE

We are interested in a model for real materials (cf. [56]) where the thermodynamic behavior, such as the specific internal energy and the pressure of the material, can be characterized by the following two-terms relations

$$e(V, T) = e_{\mathrm{ref}}(V) + e_T(V, T), \tag{3a}$$

$$p(V, T) = p_{\mathrm{ref}}(V) + \frac{\Gamma(V)}{V} e_T(V, T). \tag{3b}$$

Here $V = 1/\rho$ denotes the specific volume, T denotes the temperature, and the subscripts ref of (p, e) and T of e refer to the "reference" and "thermal" states of the variables, respectively. Note that to determine the value of T from those of V and e, we use the well-known relation in thermodynamics,

$$e - e_{\mathrm{ref}}(V) = e_T(V, T) = e_0(V) + \int_{T_0}^{T} C_V(V, T') \, dT',$$

where C_V is the specific heat at constant volume: Assume that C_V depends only on the specific volume, from the above, we simply get $e_T = C_V(T - T_0)$, yielding $T = T_0 + (e - e_{\mathrm{ref}})/C_V$. Clearly when we choose ρ and e as our nature state-variables, from (3a) and (3b), we simply get the Mie–Grüneisen equation of state (1).

Here, for simplicity, we assume that Γ is a function of V only, and takes the form

$$\Gamma(V) = \Gamma_0 \left(\frac{V}{V_0} \right)^{\alpha}, \tag{4}$$

where $\Gamma_0 = \gamma_0 - 1$ represents the Grüneisen coefficient at $V = V_0$, $\gamma_0 > 1$ is the usual definition of the ratio of specific heats, and $\alpha \in [0, 1]$ is a dimensionless parameter. Depending on the specific reference curve on which the states of the functions p_{ref} and e_{ref} lie, the explicit relation between p_{ref} and e_{ref} will be different. We next discuss two typical cases of practical importance; see [26, 55] also for some other possible instances.

2.1. Reference State along a Isentropic Locus

We begin by considering a class of materials where the thermodynamic state $(p_{\mathrm{ref}}, e_{\mathrm{ref}})$ of the model equation of state (1) lies along an isentropic locus from a centering point (p_0, e_0),

i.e., the specific entropy, denoted by S, is a constant on the curve. In this case, from the basic thermodynamics relation $de_{\text{ref}} = T\,dS - p_{\text{ref}}\,dV$ and $dS = 0$, we obtain easily the condition between p_{ref} and e_{ref} as $p_{\text{ref}}(V) = -de_{\text{ref}}(V)/dV$. Among many materials that belong to this type, in this paper we are mainly concerned with the following two sample examples which have been used quite extensively for modeling the behavior of explosives and other materials (cf. [35] for an example of solids).

(i) The Jones–Wilkins–Lee (JWL) equation of state (for gaseous explosives [9, 54]),

$$
\begin{aligned}
\Gamma(V) &= \Gamma_0 \\
e_{\text{ref}}(V) &= \frac{AV_0}{\mathcal{R}_1}\exp\left(\frac{-\mathcal{R}_1 V}{V_0}\right) + \frac{BV_0}{\mathcal{R}_2}\exp\left(\frac{-\mathcal{R}_2 V}{V_0}\right) - e_0 \\
p_{\text{ref}}(V) &= A\exp\left(\frac{-\mathcal{R}_1 V}{V_0}\right) + B\exp\left(\frac{-\mathcal{R}_2 V}{V_0}\right),
\end{aligned}
\tag{5}
$$

(ii) The Cochran–Chan (CC) equation of state (for solid explosives [6]),

$$
\begin{aligned}
\Gamma(V) &= \Gamma_0 \\
e_{\text{ref}}(V) &= \frac{-AV_0}{1-\mathcal{E}_1}\left[\left(\frac{V}{V_0}\right)^{1-\mathcal{E}_1} - 1\right] + \frac{BV_0}{1-\mathcal{E}_2}\left[\left(\frac{V}{V_0}\right)^{1-\mathcal{E}_2} - 1\right] - e_0 \\
p_{\text{ref}}(V) &= A\left(\frac{V}{V_0}\right)^{-\mathcal{E}_1} - B\left(\frac{V}{V_0}\right)^{-\mathcal{E}_2}.
\end{aligned}
\tag{6}
$$

Note that in each of these cases we have a total of seven material-dependent quantities in the description of the material property, i.e., in the former case, there are Γ_0, V_0, e_0, A, B, $\mathcal{R}_1$, and $\mathcal{R}_2$, while in the latter case, there are Γ_0, V_0, e_0, A, B, $\mathcal{E}_1$, and $\mathcal{E}_2$. Table I shows typical set of numerical values for some sample materials of interest.

2.2. *Reference State along a Hugoniot Locus*

Our next example is concerned with a popular model for solid media such as metals. In this instance, in the absence of pronounced dynamic yielding effects or phase transitions, the hydrostatic pressure is commonly expressed by the Mie–Grüneisen equation of state (1) together with a linear fit assumption for the shock velocity as a function of the particle velocity, i.e.,

$$
\sigma = c_0 + s\,u.
\tag{7}
$$

Here σ represents the shock velocity, c_0 is the zero-pressure isentropic speed of sound, and s is a dimensionless parameter which is related to the pressure derivative of the isentropic bulk modulus $K_S = \rho(\partial p/\partial\rho)|_S$ by $(\partial K_S/\partial p)|_S = 4s - 1$ (cf. [40]). By virtue of (7), it is easy to deduce that the reference curve for $(p_{\text{ref}}, e_{\text{ref}})$ is simply a single Hugoniot locus from an initial point (p_0, e_0). With this in mind, using the standard Rankine–Hugoniot jump conditions for the Euler equations (2), after some simple algebraic manipulations, we find the explicit expression for p_{ref} and e_{ref} as

$$
\begin{aligned}
p_{\text{ref}}(V) &= p_0 + \frac{c_0^2(V_0 - V)}{[V_0 - s(V_0 - V)]^2} \\
e_{\text{ref}}(V) &= e_0 + \frac{1}{2}[p_{\text{ref}}(V) + p_0](V_0 - V);
\end{aligned}
\tag{8}
$$

<div align="center">

TABLE I

**Typical Material-Dependent Quantities for Three Different Models That
Are in the Mie–Grüneisen Form (1)**

</div>

JWL EOS	ρ_0 (kg/m³)	$\mathcal{A}$ (GPa)	$\mathcal{B}$ (GPa)	$\mathcal{R}_1$	$\mathcal{R}_2$	Γ_0	α
TNT	1840	854.5	20.5	4.6	1.35	0.25	0
Water	1004	1582	−4.67	8.94	1.45	1.17	0
CC EOS	ρ_0 (kg/m³)	$\mathcal{A}$ (GPa)	$\mathcal{B}$ (GPa)	$\mathcal{E}_1$	$\mathcal{E}_2$	Γ_0	α
Copper	8900	145.67	147.75	2.99	1.99	2	0
TNT	1840	12.87	13.42	4.1	3.1	0.93	0
Shock EOS	ρ_0 (kg/m³)	c_0 (m/s)	s	Γ_0	α	p_0	e_0
Aluminum	2785	5328	1.338	2.0	1	0	0
Copper	8924	3910	1.51	1.96	1	0	0
Molybdenum	9961	4770	1.43	2.56	1	0	0
MORB	2660	2100	1.68	1.18	1	0	0
Water	1000	1483	2.0	2.0	10^{-4}	0	0

Note. Data adapted from [26, 27, 55].

see [28] for the details. Note that with Γ and (p_{ref}, e_{ref}) defined by (4) and (8), respectively, the resulting form of the Mie–Grüneisen equation of state is often called the shock wave or HOM equation of state [17, 26].

It had been discussed in detail (cf. [29]) that this shock wave equation of state has certain limitations. Nevertheless, it is observed experimentally that the model considered here is an adequate approximation for many metals, when the pressure is up to several megabars. A typical set of parameter values for metals, such as aluminum and copper, is given in Table I for the reference (cf. [27]). See [17, 40] for a more general discussion of the equation of state when (7) is replaced by a higher-order polynomial in the particle velocity.

It should be mentioned that to fulfill the conditions for the thermodynamic stability of the materials of interests, we assume that for each given physical state the speed of sound c defined by

$$
\begin{aligned}
c^2 &= \left(\frac{\partial p}{\partial \rho}\right)_S = \left(\frac{\partial p}{\partial \rho}\right)_e + \frac{p}{\rho^2}\left(\frac{\partial p}{\partial e}\right)_\rho \\
&= \left(\Gamma + 1 + \rho\frac{\Gamma'}{\Gamma}\right)\left(\frac{p - p_{ref}}{\rho}\right) + \Gamma\frac{p_{ref}}{\rho} + p'_{ref} - \Gamma\rho e'_{ref}
\end{aligned}
\tag{9}
$$

belong to a set of real numbers, where Γ', p'_{ref}, and e'_{ref} are the derivatives of Γ, p_{ref}, and e_{ref} with respect to ρ, respectively. Of course, it is both interesting and important to include the cavitation and spallation effects to materials modeled by (1) in a region where the pressure drops to a critical value. But this subject matter is a very difficult one, and is beyond the scope of this paper.

3. EQUATIONS OF MOTION

The basic governing equations in our multicomponent model consist of two parts. We use (2) as a model system that describes the motion of the fluid mixtures of the conserved variables ρ, ρu, and ρE in a multicomponent grid cell. Assume a homogeneous flow with a single velocity and pressure on grid cells that contain more than one fluid components.

From the basic physical principles of mass and energy conservations, we derive a set of effective equations for the problem-dependent material functions in those cells (see below) that can be used easily to the determination of the pressure from the equation of state. Combining these two set of the equations together with the equation of state constitutes a complete model system that is fundamental in our algorithm for numerical approximation of multicomponent problems.

To find out the aforementioned effective equations for the mixture of material quantities in a general Mie–Grüneisen equation of state (1), similar to the previous work (cf. [44, 45]), we begin by considering an interface only problem where both the pressure and particle velocity are constants in the domain, while the other variables such as the density and the material quantities are having jumps across some interfaces. In this case, from the Euler Eqs. (2), it is easy to obtain equations for the time-dependent behavior of the density and total internal energy as

$$\frac{\partial \rho}{\partial t} + u \frac{\partial \rho}{\partial x} = 0, \tag{10a}$$

$$\frac{\partial}{\partial t}(\rho e) + u \frac{\partial}{\partial x}(\rho e) = 0, \tag{10b}$$

in a respective manner. By inserting the Mie–Grüneisen equation of state (1) into (10b), we have an equation of the form

$$\frac{\partial}{\partial t}\left(\frac{p - p_{\text{ref}}}{\Gamma} + \rho e_{\text{ref}}\right) + u \frac{\partial}{\partial x}\left(\frac{p - p_{\text{ref}}}{\Gamma} + \rho e_{\text{ref}}\right) = 0 \tag{10c}$$

that is in relation to not only the pressure, but also the material quantities appearing in the functions Γ, p_{ref}, and e_{ref}.

In our algorithm, to maintain the pressure in equilibrium as it should be for our model interface only problem, we split (10c) into the following two equations for the fluid mixtures of $1/\Gamma$ and $-(p_{\text{ref}}/\Gamma) + \rho e_{\text{ref}}$ as

$$\frac{\partial}{\partial t}\left(\frac{1}{\Gamma}\right) + u \frac{\partial}{\partial x}\left(\frac{1}{\Gamma}\right) = 0, \tag{11a}$$

$$\frac{\partial}{\partial t}\left(-\frac{p_{\text{ref}}}{\Gamma} + \rho e_{\text{ref}}\right) + u \frac{\partial}{\partial x}\left(-\frac{p_{\text{ref}}}{\Gamma} + \rho e_{\text{ref}}\right) = 0, \tag{11b}$$

respectively. We emphasize that in order to have the correct pressure equilibrium in (10c) near the interfaces, these are the two key equations that should be satisfied and approximated consistently (when the problem is solved numerically) for any given expressions of Γ, p_{ref}, and e_{ref} appearing in the equation of state. As before (cf. [45]), because the solution of (11a) and (11b) would depend on not only the material quantities, but also the density, to be able to handle more general problems with shock and rarefaction waves, we need to modify each of them so that the mass-conserving behavior of the solution in the single component region can be obtained as well.

To accomplish this, consider the simpler case with (11a) as an example. Our basic approach begins with a proper smoothness assumption of the density (such as in the case of rarefaction waves), and so we may apply the chain rule from differential calculus to the

partial derivatives in (11a), yielding easily the equivalent relation

$$\frac{\partial}{\partial t}\left(\frac{1}{\Gamma}\right) + u\frac{\partial}{\partial x}\left(\frac{1}{\Gamma}\right) = -\left(\frac{\Gamma'}{\Gamma^2}\right)\left(\frac{\partial\rho}{\partial t} + u\frac{\partial\rho}{\partial x}\right).$$

Now by subtracting the term $(\rho\Gamma'/\Gamma^2)\partial u/\partial x$ from the above relation on the both sides, and using the mass conservation on the right, we arrive at an equation of the form

$$\frac{\partial}{\partial t}\left(\frac{1}{\Gamma}\right) + u\frac{\partial}{\partial x}\left(\frac{1}{\Gamma}\right) - \left(\frac{\Gamma'}{\Gamma^2}\right)\rho\frac{\partial u}{\partial x} = -\left(\frac{\Gamma'}{\Gamma^2}\right)\left(\frac{\partial\rho}{\partial t} + u\frac{\partial\rho}{\partial x} + \rho\frac{\partial u}{\partial x}\right) = 0. \quad (11c)$$

Analogously, by following the same procedure as for (11a), the modification of (11b) takes the form

$$\frac{\partial}{\partial t}\left(-\frac{p_{ref}}{\Gamma} + \rho e_{ref}\right) + u\frac{\partial}{\partial x}\left(-\frac{p_{ref}}{\Gamma} + \rho e_{ref}\right) + \left(\frac{\Gamma' p_{ref} - \Gamma p'_{ref}}{\Gamma^2} + e_{ref} + \rho e'_{ref}\right)\rho\frac{\partial u}{\partial x} = 0.$$
$$(11d)$$

Clearly, (11c) and (11d) reduce to (11a) and (11b), respectively, for a solution near the interfaces where $\partial u/\partial x = 0$, and to the same mass conservation equation of the fluid mixture for a solution near rarefaction waves where the variation of Γ'/Γ^2 is smooth. Recall that Γ', p'_{ref}, and e'_{ref} are the derivatives of Γ, p_{ref}, and e_{ref} with respect to ρ, respectively.

Note that, at each space and time, given the initial conditions for $1/\Gamma$ and $-(p_{ref}/\Gamma) + \rho e_{ref}$, to compute the solution of (11c) and (11d) would require five evaluations in total to the mixtures such as Γ', p_{ref}, p'_{ref}, e_{ref}, and e'_{ref}, from the equation of state. Here because of the strongly nonlinear coupling between the material quantities (see Section 2 for an example), from (11c) and (11d), it is not possible to come up with additional conditions for the further details of the related parameters that makes the evaluation of any of the aforementioned quantities in an explicit step. This is in contrast to the van der Waals case considered in [45], and poses some difficulties in the realization of our multicomponent algorithm for materials modeled by (1).

To get by the problems involving the extra evaluations of the terms p_{ref} and e_{ref}, in particular, one simple way to do is to divide (11d) into the following two parts:

$$\frac{\partial}{\partial t}\left(\frac{p_{ref}}{\Gamma}\right) + u\frac{\partial}{\partial x}\left(\frac{p_{ref}}{\Gamma}\right) - \rho\left(\frac{\Gamma' p_{ref} - \Gamma p'_{ref}}{\Gamma^2}\right)\frac{\partial u}{\partial x} = 0, \quad (11e)$$

$$\frac{\partial}{\partial t}(\rho e_{ref}) + u\frac{\partial}{\partial x}(\rho e_{ref}) + \rho\left(e_{ref} + \rho e'_{ref}\right)\frac{\partial u}{\partial x} = 0. \quad (11f)$$

Clearly now instead of a single equation for $-(p_{ref}/\Gamma) + \rho e_{ref}$, we have two separate ones for p_{ref}/Γ and ρe_{ref}, which together with the solutions of (11c) for Γ and the mass conservation equation in (2) for ρ are sufficient to determine p_{ref} and e_{ref} without the use of the equation of state. Of course, by doing so we still need to define Γ', p'_{ref}, and e'_{ref} so as to have a working model system.

Note that if the reference state of the Mie–Grüneisen equation of state (1) lies either along an isentropic or a shock Hugoniot locus, from the basic thermodynamic relations described in Section 2, it is an easy matter to set $e'_{ref} = p_{ref}/\rho^2$ or $e'_{ref} = [p_{ref}/\rho + p'_{ref}(\rho/\rho_0 - 1)]/(2\rho)$ in a respective manner, provided that the mixture of p'_{ref} has a proper mathematical definition

for numerical purpose also. Thus, in these two situations, to complete the model it is only the mixtures of Γ' and p'_{ref} needed to be defined. (In fact, provided that some modification of the equations is made, this is also true in a more general case where the reference state lies partially on an isentrope and partially on a Hugoniot. But we will not discuss that case here.) Although there may be other better ways, encouraged by the simplicity and also the success of the previous work for a van der Waals gas case [45], we first introduce a local model based on the volume-fraction formulation to the computation of all the remaining undefined material quantities appearing in Γ' and p'_{ref}. Then we set the mixture states of Γ' and p'_{ref} from the equation of state as in the single component case of the problem.

To be more specific, consider an m-component flow problem with materials modeled by the shock wave equation of state (8), for example, we assign the material-dependent mixtures: α, ρ_0, c_0, and s, according to an averaging operator $\mathcal{M}$ defined as follows:

$$\mathcal{M}(z) = \sum_{i=1}^{m} Y^{(i)} z^{(i)},$$

and compute $\Gamma' = -\alpha \Gamma / \rho$, $p'_{\text{ref}} = c_0^2 (1 - \eta)^2 (1 + s\eta)/(1 - s\eta)^3$ in an explicit manner. Here $Y^{(i)} \in [0, 1]$ is the volume-fraction function of the ith fluid component with a property $\sum_{i=1}^{m} Y^{(i)} = 1$, $z^{(i)}$ is a material quantity belonging to the ith component, and $\eta = 1 - (\rho_0/\rho)$. We use the evolution equation of the form

$$\frac{\partial Y^{(i)}}{\partial t} + u \frac{\partial Y^{(i)}}{\partial x} = 0,$$

for the motion of $Y^{(i)}$ (see [31] for the other possibility in choosing the equation), $i = 1, 2, \ldots, m - 1$, where u is the underlying particle velocity of the fluid mixture, and set $Y^{(m)} = 1 - \sum_{i=1}^{m-1} Y^{(i)}$. In summary, with the Mie–Grüneisen equation of state (1), the multicomponent model we proposed consists of the following system of equations,

$$\frac{\partial \rho}{\partial t} + \frac{\partial}{\partial x}(\rho u) = 0$$

$$\frac{\partial}{\partial t}(\rho u) + \frac{\partial}{\partial x}(\rho u^2 + p) = 0$$

$$\frac{\partial}{\partial t}(\rho E) + \frac{\partial}{\partial x}(\rho E u + pu) = 0$$

$$\frac{\partial}{\partial t}\left(\frac{1}{\Gamma}\right) + u\frac{\partial}{\partial x}\left(\frac{1}{\Gamma}\right) - \rho\left(\frac{\Gamma'}{\Gamma^2}\right)\frac{\partial u}{\partial x} = 0 \qquad (12)$$

$$\frac{\partial}{\partial t}\left(\frac{p_{\text{ref}}}{\Gamma}\right) + u\frac{\partial}{\partial x}\left(\frac{p_{\text{ref}}}{\Gamma}\right) - \rho\left(\frac{\Gamma' p_{\text{ref}} - \Gamma p'_{\text{ref}}}{\Gamma^2}\right)\frac{\partial u}{\partial x} = 0$$

$$\frac{\partial}{\partial t}(\rho e_{\text{ref}}) + u\frac{\partial}{\partial x}(\rho e_{\text{ref}}) + \rho(e_{\text{ref}} + \rho e'_{\text{ref}})\frac{\partial u}{\partial x} = 0$$

$$\frac{\partial Y^{(i)}}{\partial t} + u\frac{\partial Y^{(i)}}{\partial x} = 0, \quad \text{for } i = 1, 2, \ldots, m - 1.$$

This gives us a system of $m + 5$ equations in total that is independent of the number of material quantities involved in the equation of state (e.g., there are seven of them in (5) or (6)), for an m-component flow problem; $m \geq 1$. It is easy to see that in this system the first

three are the Euler equations which are used to make certain the conservation of the basic fluid mixtures: ρ, ρu, and ρE, while the remaining ones are the effective equations that are introduced to ensure the correct mixing of the problem-dependent material variables near the interfaces. With a system written in this way, there is no problem to compute the pressure from the equation of state

$$p = \left[(\rho E) - \frac{(\rho u)^2}{2\rho} + \left(\frac{p_{\mathrm{ref}}}{\Gamma} \right) - (\rho e_{\mathrm{ref}}) \right] \Big/ \left(\frac{1}{\Gamma} \right).$$

The initialization of the state variables in (12) for fluid-mixture cells can be made in a standard way as described in [45] for numerical simulation.

Note that, when $m = 1$ (single component flow), the effect to the introduction of the equations for $1/\Gamma$, p_{ref}/Γ, and ρe_{ref} in the model is to reduce extra equation-of-state computations in a numerical method to the least possible amount. It is easy to see that our multicomponent model is a hyperbolic system by first writing (12) in a quasi-linear system of equations

$$\frac{\partial q}{\partial t} + A(q) \frac{\partial q}{\partial x} = 0. \tag{13}$$

Here, for simplicity, in a two-component version of the model, we have the state vector q and the matrix A defined by

$$q = \left[\rho, \rho u, \rho E, \frac{1}{\Gamma}, \frac{p_{\mathrm{ref}}}{\Gamma}, \rho e_{\mathrm{ref}}, Y \right]^T$$

and

$$A = \begin{bmatrix} 0 & 1 & 0 & 0 & 0 & 0 & 0 \\ K - u^2 & u(2 - \Gamma) & \Gamma & -p\Gamma & -\Gamma & \Gamma & 0 \\ u(K - H) & H - u^2\Gamma & u(\Gamma + 1) & -up\Gamma & -u\Gamma & u\Gamma & 0 \\ -\varphi u & \varphi & 0 & u & 0 & 0 & 0 \\ -\chi u & \chi & 0 & 0 & u & 0 & 0 \\ -\psi u & \psi & 0 & 0 & 0 & u & 0 \\ 0 & 0 & 0 & 0 & 0 & 0 & u \end{bmatrix}.$$

We then compute the eigen-structure of the matrix A. It is a straightforward to show that for each variables q defined in the region of thermodynamic stability the eigen-structure of the matrix A possesses real eigenvalues

$$\Lambda = \mathrm{diag}(\lambda_1, \lambda_2, \ldots, \lambda_7) = \mathrm{diag}(u - c, u, u + c, u, \ldots, u) \tag{14a}$$

and a complete set of eigenvectors of the form

$$R = (r_1, r_2, \ldots, r_7) = \begin{bmatrix} 1 & 1 & 1 & 0 & 0 & 0 & 0 \\ u - c & u & u + c & 0 & 0 & 0 & 0 \\ H - uc & u^2/2 & H + uc & p & 1 & -1 & 0 \\ \varphi & 0 & \varphi & 1 & 0 & 0 & 0 \\ \chi & 0 & \chi & 0 & 1 & 0 & 0 \\ \psi & 0 & \psi & 0 & 0 & 1 & 0 \\ 0 & 0 & 0 & 0 & 0 & 0 & 1 \end{bmatrix} \tag{14b}$$

with $Ar_k = \lambda_k r_k$. Here $K = \Gamma u^2/2$, $H = E + (p/\rho)$, $\varphi = -\Gamma'/\Gamma^2$, $\chi = (\Gamma p'_{\text{ref}} - \Gamma' p_{\text{ref}})/\Gamma^2$, and $\psi = e_{\text{ref}} + \rho e'_{\text{ref}}$. Regarding discontinuous solutions of the system, such as shock waves or contact discontinuities, it is not difficult to show that (12) has the usual form of the Rankine–Hugoniot jump conditions across the waves; see Section 4.1 for more details.

4. NUMERICAL METHODS

To find approximate solutions of our model system (12) for multicomponent problems, we use a high-resolution wave propagation method developed by LeVeque [20, 23] for general hyperbolic systems of partial differential equations. This method is a variant of the fluctuation-and-signal scheme of Roe [37, 38] in that we solve the Riemann problems at each cell interface, and use the resulting waves (i.e., discontinuities moving at constant speeds) to update the solutions in neighboring grid cells. To achieve high resolution, we introduce slopes and limiters to the method as in many other high resolution schemes for conservation laws [21, 50].

4.1. Roe Riemann Solver

Clearly, one of the major steps in our multicomponent algorithm is the numerical resolution of the Riemann problem at each cell interface. Here, with materials characterized by the Mie–Grüneisen equation of state (1), this amounts to solving the nonlinear system (12) with piecewise constant data q_L and q_R to the left and right of the interface. It is well-known that, except under certain extreme conditions (cf. [31, 34, 55, 56]), the solution of this Riemann problem would consist of two genuinely nonlinear waves, such as shock and rarefaction, and a linearly degenerate wave (contact discontinuity); this is just like the Riemann problem for a perfect gas (cf. [48]). In Fig. 1, we plot a typical solution structure and the variables involved in the Riemann problem considered here. Because in general it
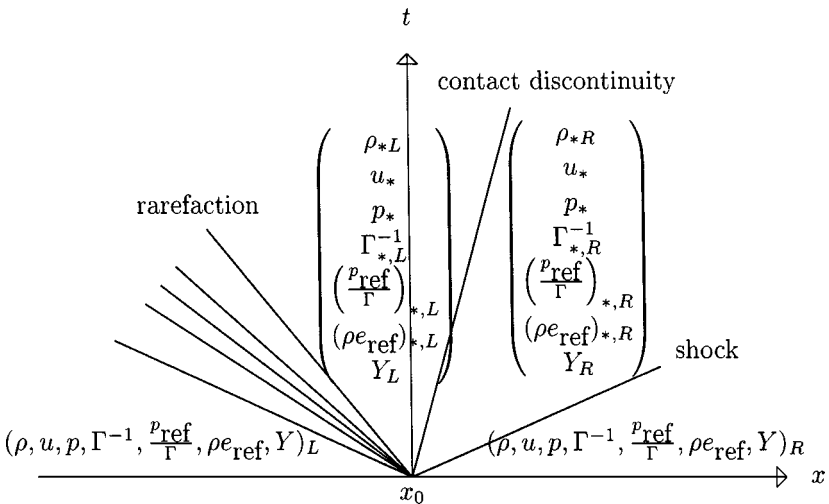
FIG. 1. Typical solution structure of the Riemann problem for our multicomponent model discussed in Section 3. The key step in obtaining this solution is to find the midstate (u_*, p_*) in the $u - p$ phase plane. In general, it is a difficult task to do both exactly and efficiently.

is too complicated to solve the problem exactly, even in the single component case for real materials (cf. [8, 36, 43]), we discuss an approximate Riemann solver of Roe; see [31, 36] for another approach based on the two-shock approximation.

In a Roe's approximate Riemann solver, we replace the nonlinear Riemann problem mentioned above by a linear problem as

$$\frac{\partial q}{\partial t} + \hat{A}(q_L, q_R) \frac{\partial q}{\partial x} = 0, \qquad q(x, 0) = \begin{cases} q_L & \text{for } x < x_0 \\ q_R & \text{for } x > x_0, \end{cases} \tag{15}$$

where $\hat{A}(q_L, q_R)$ is a constant matrix that depends on the initial data and is a local linearization of the matrix A in (13) about an average state. To find that matrix, as it is often done in many other Roe solvers (cf. [5, 14, 15]), we want to seek an average state that the difference of the fluxes in the conservation part of (12) (i.e., the first three equations of the system) are equal to the respective first-order approximation of the flux differences. That is

$$\Delta \mathcal{F}^{(i)} = (\mathcal{F}_R - \mathcal{F}_L)^{(i)} = [\hat{A}(q_L, q_R)(q_R - q_L)]^{(i)} = [\hat{A}(q_L, q_R)\Delta q]^{(i)},$$

for $i = 1, 2, 3$, where $\mathcal{F} \in \mathbb{R}^3$ is the usual definition of the fluxes for conservation laws, and $\Delta \mathcal{F}^{(i)}$ is the ith component of $\Delta \mathcal{F}$. With that, it is a straightforward matter to obtain the results for $\hat{u}$ and $\hat{H}$ by the standard "Roe-averaging" approach, i.e., for a given pair (ρ_L, ρ_R), the average state for a quantity z is defined by

$$\hat{z} = \frac{\sqrt{\rho_L} z_L + \sqrt{\rho_R} z_R}{\sqrt{\rho_L} + \sqrt{\rho_R}}. \tag{16}$$

Note that in the process of the derivation, as in [44, 45], we have chosen the averages $\widehat{(1/\Gamma)}$ and $\widehat{(p/\Gamma)}$ based on (16) so that the expression

$$\Delta p = \left[\widehat{\left(\frac{1}{\Gamma}\right)} \Delta \left(\frac{p}{\Gamma}\right) - \widehat{\left(\frac{p}{\Gamma}\right)} \Delta \left(\frac{1}{\Gamma}\right) \right] \bigg/ \widehat{\left(\frac{1}{\Gamma}\right)}^2$$

is satisfied approximately (cf. [33] for an review of the other up-to-date approaches for real gases). With that we set $\hat{p} = \widehat{(p/\Gamma)}/\widehat{(1/\Gamma)}$ and $\hat{\Gamma} = 1/\widehat{(1/\Gamma)}$. To finish the construction of $\hat{A}(q_L, q_R)$, we still need to find the averages of φ, χ, and ψ. Since there is no unique way to do so, we might as well compute them using the Roe-average (16) also. It is our experience that the set of average states described here is a reasonable one to use for many practical multicomponent problems (see numerical results present in Section 5) as long as the flow condition is not too extreme (i.e., with very large density and pressure ratios) across the interfaces, (cf. [11, 45] for more discussions and the possible cures for that matters).

In contrast to the solution structure for a nonlinear Riemann problem (see Fig. 1), the solution of the linear problem (15) consists of seven discontinuities propagating at constant speeds (for a two-component system of seven equations). The jump across each discontinuity is a multiple of the eigenvector of the matrix $\hat{A}$, and the propagating speed is the corresponding eigenvalue. We thus have

$$\Delta q = q_R - q_L = \sum_{k=1}^{7} \hat{\alpha}_k \hat{r}_k, \tag{17}$$

where $\hat{r}_k$ is the kth eigenvector of $\hat{A}$; see (14a) and (14b). The scalar $\hat{\alpha}_k$ gives the strength across the discontinuity that can be determined easily from (17). We find

$$\hat{\alpha}_2 = \Delta q^{(1)} + \frac{\hat{\Gamma}}{\hat{c}^2}\left[-\frac{\hat{u}^2}{2}\Delta q^{(1)} + \hat{u}\Delta q^{(2)} - \Delta q^{(3)} + \hat{p}\Delta q^{(4)} - \Delta q^{(5)} + \Delta q^{(6)}\right],$$

$$\hat{\alpha}_3 = \frac{1}{2\hat{c}}\left[(\hat{c}-\hat{u})\Delta q^{(1)} + \Delta q^{(2)} - \hat{c}\hat{\alpha}_2\right], \quad \hat{\alpha}_1 = \Delta q^{(1)} - \hat{\alpha}_2 - \hat{\alpha}_3,$$

$$\hat{\alpha}_4 = \Delta q^{(4)} - \hat{\varphi}(\Delta\rho - \hat{\alpha}_2), \qquad\qquad \hat{\alpha}_5 = \Delta q^{(5)} - \hat{\chi}(\Delta\rho - \hat{\alpha}_2), \qquad (18)$$

$$\hat{\alpha}_6 = \Delta q^{(6)} - \hat{\psi}(\Delta\rho - \hat{\alpha}_2), \qquad\qquad \hat{\alpha}_7 = \Delta q^{(7)},$$

where $\hat{c} = \sqrt{\hat{\Gamma}[\hat{H} - (\hat{u}^2/2) + \hat{\chi} - \hat{\psi}]}$ is the speed of sound.

Notice that in this Riemann solution, except the discontinuities for $\hat{\lambda}_1 = \hat{u} - \hat{c}$ and $\hat{\lambda}_3 = \hat{u} + \hat{c}$, all the other discontinuities (five of them) are propagating at the same speed $\hat{u}$. For practical purposes, we may view these discontinuities as a single one with the operator $\mathcal{W}_2$ defined by combining all the jumps across the $\hat{\lambda}_2$ wave family, i.e., set $\mathcal{W}_2 = \hat{\alpha}_2\hat{r}_2 + \sum_{k=4}^{7}\hat{\alpha}_k\hat{r}_k$. With this notation, we also write $\mathcal{W}_k = \hat{\alpha}_k\hat{r}_k$ to represent the jump across the k-wave for $k = 1$ or 3. Thus, without causing any confusion, we may assume that the wave family in total is 3 for the solution of this Riemann problem.

4.2. High-Resolution Wave Propagation Scheme

Consider a uniform grid with fixed mesh spacing $\triangle x$, for example. We use a standard finite-volume formulation in which the value Q_j^n approximates the cell average of the solution over the grid cell $[x_j, x_{j+1}]$ at time t_n:

$$Q_j^n \approx \frac{1}{\Delta x}\int_{x_j}^{x_{j+1}} q(x, t_n)\,dx.$$

The time step from the current time t_n to the next t_{n+1} is denoted by Δt.

In this numerical discretization setup, a first-order accurate version of the method in wave-propagation form is a Godunov-type scheme that can be written as

$$Q_j^{n+1} = Q_j^n - \frac{\Delta t}{\Delta x}\sum_{k=1}^{m_w}(\lambda_k^-\mathcal{W}_k)_{j+1}^n + (\lambda_k^+\mathcal{W}_k)_j^n, \qquad (19)$$

where $\lambda_k \in \mathbb{R}$ and $\mathcal{W}_k \in \mathbb{R}^m$ are solutions of the kth wave family, for $k = 1, 2, \dots, m_w$, obtained from solving the Riemann problems at cell interfaces x_j and x_{j+1}; see Section 4.1. As usual, we define $\lambda^- = \min(\lambda, 0)$ and $\lambda^+ = \max(\lambda, 0)$. Clearly, the method belongs to a class of upwind schemes (cf. [15, 21]), and by following the same procedure as described in [45], it is quasi-conservative in the sense that when applying the method to (12) not only the conservation equations but also the transport equations are approximated in a consistent manner by the method with the chosen Riemann solver.

To achieve high resolution in this method, we begin by introducing correction waves in a piecewise-linear form with zero mean value. We then propagate each wave over the time step Δt, and update the cell averages it overlaps. Without going into the detail here

(cf. [24]), with the corrections, (19) is modified by

$$Q_j^{n+1} := Q_j^{n+1} - \frac{\Delta t}{2\Delta x} \sum_{k=1}^{m_w} \left[|\lambda_k| \left(1 - |\lambda_k| \frac{\Delta t}{\Delta x} \right) \mathcal{W}_k \right]_{j+1}^n - \left[|\lambda_k| \left(1 - |\lambda_k| \frac{\Delta t}{\Delta x} \right) \mathcal{W}_k \right]_j^n. \quad (20)$$

It is important to mention that, in practice, the jump of each wave in the above formula should be limited by using a "slope-limiter" (cf. [21]) to avoid unnecessary fluctuations near discontinuities. We want to do this by replacing each $\mathcal{W}_k$ in (20) with a limited value $\widetilde{\mathcal{W}}_k$ obtained by comparing $\mathcal{W}_k$ with the corresponding $\mathcal{W}_k$ from the neighboring Riemann problem to the left (if $\lambda_k > 0$) or to the right (if $\lambda_k < 0$).

Now with the use of the Roe solver to the computations, it is quite common to limit over each strength of the wave $\hat{\alpha}_{kj}$ *via* a limiter function ϕ (e.g., by using the minmod function $\phi(\theta) = \max(0, \min(1, \theta))$ or some others as discussed in [50]), and set

$$\tilde{\alpha}_{kj} = \phi(\theta_{kj}) \hat{\alpha}_{kj} \quad \text{with} \quad \theta_{kj} = \frac{\hat{\alpha}_{kJ}}{\hat{\alpha}_{kj}}, \quad J = \begin{cases} j-1 & \text{if} \quad \hat{\lambda}_{kj} \geq 0 \\ j+1 & \text{if} \quad \hat{\lambda}_{kj} < 0, \end{cases} \quad (21)$$

for $k = 1, 2, \ldots, 7$ (cf. [15, 22, 23]). In this approach, we then replace the waves in (20),

$$(\mathcal{W}_1, \mathcal{W}_2, \mathcal{W}_3) = \left(\hat{\alpha}_1 \hat{r}_1, \hat{\alpha}_2 \hat{r}_2 + \sum_{k=4}^{7} \hat{\alpha}_k \hat{r}_k, \hat{\alpha}_3 \hat{r}_3 \right),$$

by a limited version as

$$(\widetilde{\mathcal{W}}_1, \widetilde{\mathcal{W}}_2, \widetilde{\mathcal{W}}_3) = \left(\tilde{\alpha}_1 \hat{r}_1, \tilde{\alpha}_2 \hat{r}_2 + \sum_{k=4}^{7} \tilde{\alpha}_k \hat{r}_k, \tilde{\alpha}_3 \hat{r}_3 \right).$$

It is not difficult to show that for the interface only problem we again have the required pressure equilibrium that is independent of the limiter being employed to the high-resolution method (20). Moreover, we obtain a better resolution of the result as compared to the first-order result. Concerning stability of the method, it is observed numerically that the method is stable under the usual CFL (Courant–Friedrichs–Lewy) condition for hyperbolic systems of conservation laws; see Section 5 for an example.

5. NUMERICAL RESULTS IN ONE DIMENSION

We now present some sample numerical results obtained using our multicomponent algorithm with the Roe solver described in Section 4.

5.1. *Single-Component Case*

As a preliminary, we begin by showing results for problems with only a single fluid component presence in the problem formulation.

EXAMPLE 5.1.   Our first test problem is a Riemann problem in a shock tube with the material inside the tube modeled by the Jones–Wilkins–Lee equation of state (5). For comparison purposes, we take the similar initial data as studied by Rider [36], where on the
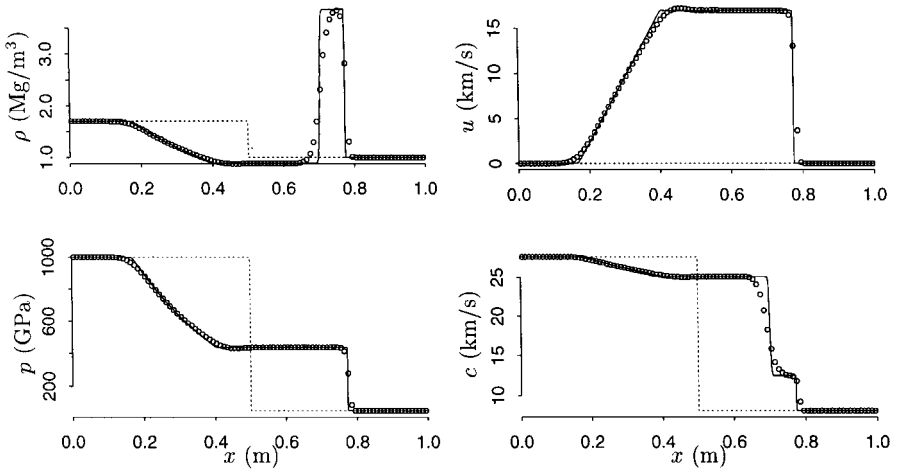
FIG. 2. High-resolution results for a single component Riemann problem with the gaseous explosives at time $t = 12 \, \mu s$. The solid line is the fine grid solution computed by $\Delta x = 1/2000$, and the points show the solution with $\Delta x = 1/100$. The dashed line in each subplot is the initial condition at time $t = 0$. The gaseous explosive is modeled by the Jones–Wilkins–Lee equation of state (5).

left of the interface, $0 \le x < 1/2$ m, we have

$$(\rho, u, p, e_0)_L = (1700 \text{ kg/m}^3, 0 \text{ m/s}, 10^{12} \text{ Pa}, 0 \text{ kJ/kg}),$$

and on the right of the interface, $1/2$ m $\le x \le 1$ m, we have

$$(\rho, u, p, e_0)_R = (1000 \text{ kg/m}^3, 0 \text{ m/s}, 5 \times 10^{10} \text{ Pa}, 0 \text{ kJ/kg}).$$

In this problem, the seven material-dependent quantities: ρ_0, $\mathcal{A}$, $\mathcal{B}$, $\mathcal{R}_1$, $\mathcal{R}_2$, Γ_0, and α, have been chosen for the product gases of the explosive TNT as given in Table I.

In Fig. 2, we show results for the density, velocity, pressure, and the speed of sound at time $t = 12 \, \mu s$, where the test has been carried out by using the high-resolution method with the MINMOD limiter, the Courant number $\mu = 0.9$, and the mesh size $\Delta x = 1/100$. By comparing the computed solution with the fine grid solution obtained using the same method but $\Delta x = 1/2000$, we observe good agreement in the region of rarefaction wave where the flow is smooth, and reasonable resolution in the region of shock and contact discontinuity where the flow is not smooth (judging from the approximate location and the monotonicity of the solution profile for the discontinuity). In addition, it is easy to make comparisons and see that our solution agrees quite well with the result present in [36] where a MUSCL-type scheme with an approximate Riemann solver based on the two-shock approximation was used in the computation.

EXAMPLE 5.2. We are next concerned with an impact problem in which a precompressed semi-infinite aluminum slab at rest with $(\rho, p) = (4000 \text{ kg/m}^3, 7.93 \times 10^9 \text{ Pa})$ is being hit by an ambient aluminum slab traveling at the speed 2 km/s from the right to the left with the reference state $(\rho, p) = (\rho_0, p_0)$. As in [29, 31, 36] and references therein, we use the popular shock wave equation of state (8) to model the thermodynamical behavior of the aluminum; see Table I for the numerical values of the material constants: ρ_0, c_0, s, Γ_0, and α.

In this setup, it is not difficult to show that the exact solution of this problem would consist of a leftward going shock wave to the stationary aluminum, a material interface,
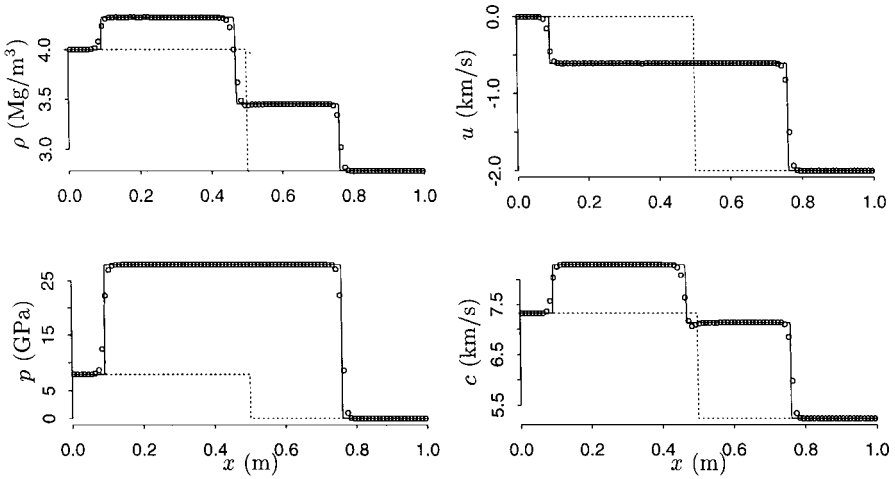
FIG. 3. High-resolution results for a single component impact problem with two aluminum slabs at time $t = 50\,\mu s$. The aluminum is modeled by the shock wave equation of state (8). The graphs of the solutions are displayed in the same manner as in Fig. 2.

and a rightward going shock wave to the moving aluminum. Figure 3 shows the numerical result for this problem at time $t = 50\,\mu s$. As compared to the fine grid solution, which is a good approximation to the exact solution, it is clear that our result gives the correct solution behavior of this problem; see [36] also for a similar calculation. Here the computation was performed in the same manner as in Example 5.1, where the initial point of the projectile impact was set at the center of a meter-wide computational domain.

5.2. Multicomponent Case

We now show results for examples with more than one fluid component in the problem formulation.

EXAMPLE 5.3. To begin, we are interested in a two-component impact problem of Saurel and Abgrall [41]. Initially, under the atmospheric condition (i.e., with uniform pressure $p_0 = 1$ atm and temperature $T_0 = 300$ K throughout the domain), there is a rightward going copper plate with the speed $u = 1500$ m/s interacting with a solid explosive (considered as an inert material) at rest on the right of the plate. In this problem, to model the material properties of the copper and (solid) explosive, we use the same Cochran–Chan equation of state (6), but with a different set of material-dependent quantities for each of them, see numerical values given in Table I.

As in Example 5.2, the exact solution of this impact problem is composed of a leftward-going shock wave to the copper, a rightward-going shock waves to the inert explosive, and a material interface lying in between that separates these different materials. We run this problem using exactly the same method as performed in the previous examples for single component flow, and show the resulting solution in Fig. 4 at time $t = 85\,\mu s$ for the density, velocity, pressure, and the thermal internal energy. By comparing the computed solution with the fine grid one obtained using the same method but $\Delta x = 1/2000$, we observe reasonable behavior of the solution with the correct shock speeds and free of spurious oscillations in the pressure near the interface. Checking our result with the displayed solution appearing
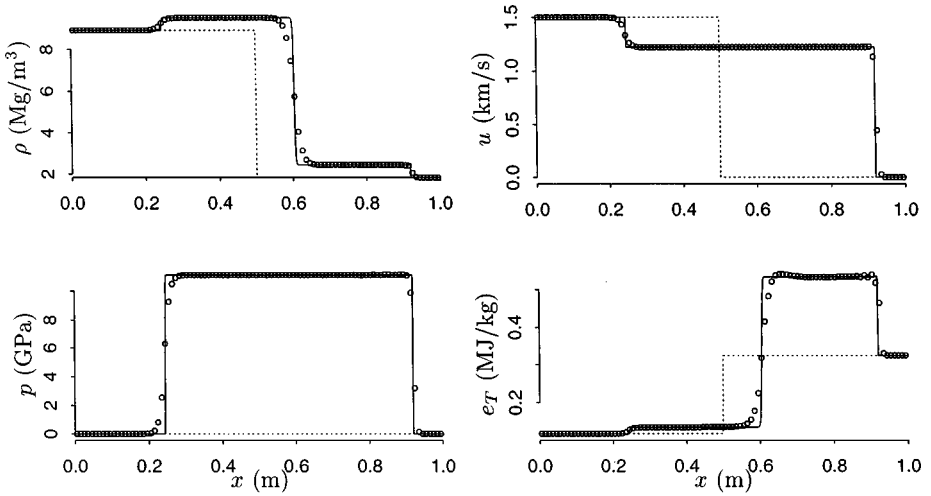
FIG. 4. High-resolution results for a two-component (solid explosive-copper) impact problem at time $t = 85\,\mu$s. The solid line is the fine grid solution computed by $\Delta x = 1/2000$, and the points show the solution with $\Delta x = 1/100$. The dashed line in each subplot is the initial condition at time $t = 0$. Both the solid explosive and copper are modeled by the Cochran–Chan equation of state (6), but with a different set of material quantities for each of them.

in [41] with the same mesh size $\Delta x = 1/100$, we find excellent agreement in the density, pressure, and velocity. Clearly, for detonation problems, it is often necessary to report the solution of the temperature T as well. As we have seen in the figure (see Fig. 5 also), the algorithm did quite a good job to the resolution of thermal internal energy e_T which can be computed directly from the variables obtained in the algorithm, i.e., $e_T = (p - p_{\mathrm{ref}})/(\rho\Gamma)$. To go one step further to T by $T = e_T/C_V$, we need to do some postprocessing work for the fluid mixture C_V. Although there are many ways to get C_V, say by using the volume-fraction
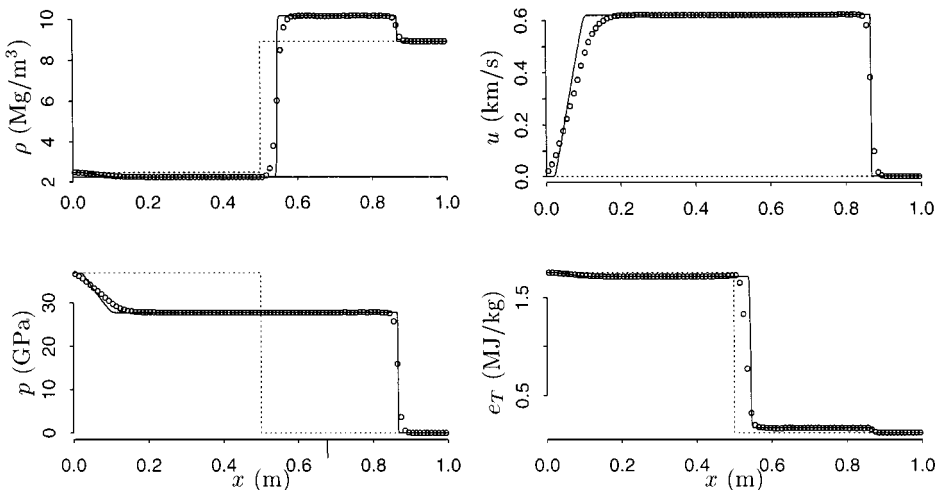
FIG. 5. High-resolution results for a two-component (gaseous explosive–copper) Riemann problem at time $t = 73\,\mu$s. The gaseous explosive is modeled by the Jones–Wilkins–Lee equation of state (5), while the copper is modeled by the Cochran–Chan equation of state (6). The graphs of the solutions are displayed in the same manner as in Fig. 4.

function, for example, this is not really in the heart of the whole algorithm, and so the plot of the temperature is not shown here. Note that, we have $C_V = 393$ and $1087 \, \text{J/(kg} \cdot \text{K)}$ for copper and explosive, respectively.

EXAMPLE 5.4.   Our next example concerns a two-component Riemann problem of Saurel and Abgrall [41] that involves the interaction of gaseous detonation products with a copper plate. In this test, as in Example 5.3, copper is modeled by the Cochran–Chan equation of state (6), while the detonation products are modeled by the widely employed Jones–Wilkins–Lee equation of state (5). Initially, on the left when $x \in [0, 0.5]$m, we have the detonation product with the data

$$(\rho, u, p, e_0)_L = (2485.37 \text{ kg/m}^3, 0, 3.7 \times 10^{10} \text{ Pa}, \ 8149.158 \text{ kJ/kg}),$$

and on the right when $x \in [0.5, 1]$m, we have the copper with data

$$(\rho, u, p, e_0)_R = (8900 \text{ kg/m}^3, 0, 10^5 \text{ Pa}, \ 117.9 \text{ kJ/kg}).$$

We note that the data on the left is at the Chapman–Jouget state (see [41] for the details), while the data on the right is at the usual atmospheric conditions. In Table I, we list the material quantities of these two substances to this run. For this problem, it is known that the exact solution consists of a shock wave moving to the right in the copper and a rarefaction wave propagating to the left in the explosive; see [41].

To solve this problem numerically, we need to define a hybrid version of the equation of state that is necessary in the algorithm for the numerical mixing between these two different materials. This can be done by following the same approach as described in [45] for a case with the mixing between stiffened and van der Waals gases, yielding easily a Mie–Grüneisen equation of state of the form

$$p(\rho, e) = \tilde{p}_{\text{ref}}(\rho) + \tilde{\Gamma}\rho[e - \tilde{e}_{\text{ref}}(\rho)] \tag{22}$$

for the copper-explosive mixture, where $\tilde{p}_{\text{ref}} = p_{\text{ref}}^{(\text{JWL})} + p_{\text{ref}}^{(\text{CC})}$ and $\tilde{e}_{\text{ref}} = e_{\text{ref}}^{(\text{JWL})} + e_{\text{ref}}^{(\text{CC})}$ are defined by simply combining the two different p_{ref} and e_{ref} from (5) and (6) into one, respectively, and $\tilde{\Gamma} = \Gamma_0$. Here the computation was performed in the same way as before, and the results are shown in Fig. 5 at time $t = 73 \, \mu$s for the variables ρ, u, p, and e_T also. Comparing our solution with the one shown in [41] using a two-phase flow solver, we again observe good agreement for this problem.

EXAMPLE 5.5.   To end this section, we test our algorithm for a model shock-contact problem that involves the interaction of a shock wave in molybdenum and an encapsulated MORB (Mid-Ocean Ridge Basalt) liquid (this problem is motivated by a two-dimensional test of Miller and Puckett [31]). The initial condition is composed of a stationary (molybdenum-MORB) interface at $x = 0.6$ m and a rightward going Mach 1.163 shock wave in molybdenum at $x = 0.4$ m traveling from left to right in a shock tube of unit length. The material on the right of the interface is a MORB liquid modeled by the shock wave equation of state (8) with the data

$$(\rho, u, p, e_0)_R = (2260 \text{ kg/m}^3, 0 \text{ m/s}, 0 \text{ Pa}, 0 \text{ kJ/kg}),$$

and the material on the left of the interface (i.e., on the middle and the preshock state) is molybdenum modeled by the shock wave equation of state also with data

$$(\rho, u, p, e_0)_M = (9961 \text{ kg/m}^3, 0 \text{ m/s}, 0 \text{ Pa}, 0 \text{ kJ/kg}).$$
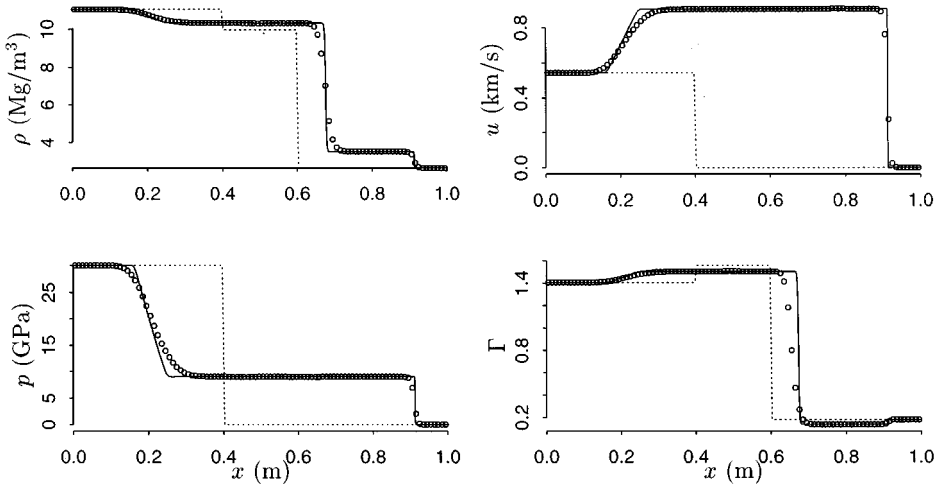
FIG. 6. High-resolution results for a shock wave in molybdenum interacting with an encapsulated MORB liquid at time $120\,\mu s$. The solid line is the fine grid solution computed by $\Delta x = 1/2000$, and the points show the solution with $\Delta x = 1/100$. The dashed line in each subplot is the initial condition at time $t = 0$. Both the molybdenum and MORB are modeled by the shock wave equation of state (8), but with different material constants for each of them.

The state behind the shock in the molybdenum is

$$(\rho, u, p, e_0)_L = (11042 \text{ kg/m}^3, 543 \text{ m/s}, 3 \times 10^{10} \text{ Pa}, 0 \text{ kJ/kg}),$$

see the dashed line shown in Fig. 6 for illustration. We note that this gives us one example in which the (molybdenum-MORB) interface is accelerated by a shock wave coming from the heavy-fluid to the light-fluid region, and it is known that the resulting wave pattern after the interaction would consist of a transmitted shock wave, an interface, and a reflected rarefaction wave (cf. [4, 16]).

Numerical results for this problem are shown in Fig. 6 at time $t = 120\,\mu s$ for the states ρ, u, p, and Γ. Clearly, we observe sensible resolution and convergence of the solution structure as the mesh is refined. Note that because of the passage of the transmitted shock wave, the MORB liquid is compressed, yielding the increase of the density, velocity, and pressure. A two-dimensional version of this problem will be considered in Section 6.1.

6. EXTENSION TO MULTIPLE DIMENSIONS

The multidimensional version of our model system (12) for compressible multicomponent problems with the Mie–Grüneisen equation of state (1) takes the form

$$\frac{\partial \rho}{\partial t} + \sum_{j=1}^{N} \frac{\partial}{\partial x_j} (\rho u_j) = 0$$

$$\frac{\partial}{\partial t} (\rho u_i) + \sum_{j=1}^{N} \frac{\partial}{\partial x_j} \left(\rho u_i u_j + \delta^{ij} p \right) = 0 \quad \text{for } i = 1, 2, \ldots, N$$

$$\frac{\partial}{\partial t}(\rho E) + \sum_{j=1}^{N} \frac{\partial}{\partial x_j}(\rho E u_j + p u_j) = 0$$

$$\frac{\partial}{\partial t}\left(\frac{1}{\Gamma}\right) + \sum_{j=1}^{N}\left[u_j \frac{\partial}{\partial x_j}\left(\frac{1}{\Gamma}\right) - \rho\left(\frac{\Gamma'}{\Gamma^2}\right)\frac{\partial u_j}{\partial x_j}\right] = 0 \qquad (23)$$

$$\frac{\partial}{\partial t}\left(\frac{p_{\text{ref}}}{\Gamma}\right) + \sum_{j=1}^{N}\left[u_j \frac{\partial}{\partial x_j}\left(\frac{p_{\text{ref}}}{\Gamma}\right) - \rho\left(\frac{\Gamma' p_{\text{ref}} - \Gamma p'_{\text{ref}}}{\Gamma^2}\right)\frac{\partial u_j}{\partial x_j}\right] = 0$$

$$\frac{\partial}{\partial t}(\rho e_{\text{ref}}) + \sum_{j=1}^{N}\left[u_j \frac{\partial}{\partial x_j}(\rho e_{\text{ref}}) + \rho(e_{\text{ref}} + \rho e'_{\text{ref}})\frac{\partial u_j}{\partial x_j}\right] = 0$$

$$\frac{\partial Y^{(i)}}{\partial t} + \sum_{j=1}^{N} u_j \frac{\partial Y^{(i)}}{\partial x_j} = 0, \quad \text{for } i = 1, 2, \ldots, m-1.$$

Here N is the number of spatial dimensions ($N = 2$ or 3, for example), u_j is the particle velocity in the x_j-direction, δ^{ij} is the Kronecker delta that takes the value 1 when $i = j$, but equals to 0 otherwise, and $E = e + \sum_{j=1}^{N} u_j^2/2$. As before (cf. [44, 45] and Section 3), in the model, the first $N + 2$ components are simply the Euler equations in N dimensions that describe the conservation of mass, momenta in the x_j-direction, for $j = 1, 2, \cdots, N$, and energy of the problem. The next three are the effective equations that are derived for the problem-dependent material quantities. We include the transport equation for the volume-fraction functions $Y^{(i)}$, for $i = 1, 2, \ldots, m-1$, in the model for the evaluation of Γ' and p'_{ref}. In the algorithm, we again compute the pressure from the equation of state at all space and time,

$$p = \left[(\rho E) - \frac{\sum_{j=1}^{N}(\rho u_j)^2}{2\rho} + \left(\frac{p_{\text{ref}}}{\Gamma}\right) - (\rho e_{\text{ref}})\right] \Big/ \left(\frac{1}{\Gamma}\right).$$

Note that, for any given N, if the state variables of the flow are all in the region of the thermodynamic stability (this is the case we are interested in here), it is not difficult to show that (23) is a hyperbolic system in the sense that any linear combination of the matrices A_j, $j = 1, 2, \ldots, N$, appearing in the quasi-linear form of the equations

$$\frac{\partial q}{\partial t} + \sum_{j=1}^{N} A_j(q)\frac{\partial q}{\partial x_j} = 0 \qquad (24)$$

has real eigenvalues and a complete set of eigenvectors. Consider the most general three-dimensional case $N = 3$ and for a two-component $m = 2$ problem, for example. We then have the state vector q in (24) defined by

$$q = \left[\rho, \ \rho u_1, \ \rho u_2, \ \rho u_3, \ \rho E, \ \frac{1}{\Gamma}, \ \frac{p_{\text{ref}}}{\Gamma}, \ \rho e_{\text{ref}}, \ Y\right]^T,$$

and the matrices A_j, for $j = 1, 2, 3$, defined by

$$
A_1 = \begin{bmatrix}
0 & 1 & 0 & 0 & 0 & 0 & 0 & 0 & 0 \\
K - u_1^2 & u_1(2 - \Gamma) & -u_2\Gamma & -u_3\Gamma & \Gamma & -p\Gamma & -\Gamma & \Gamma & 0 \\
-u_1 u_2 & u_2 & u_1 & 0 & 0 & 0 & 0 & 0 & 0 \\
-u_1 u_3 & u_3 & 0 & u_1 & 0 & 0 & 0 & 0 & 0 \\
u_1(K - H) & H - u_1^2\Gamma & -u_1 u_2\Gamma & -u_1 u_3\Gamma & u_1(\Gamma + 1) & -u_1 p\Gamma & -u_1\Gamma & u_1\Gamma & 0 \\
-\varphi u_1 & \varphi & 0 & 0 & 0 & u_1 & 0 & 0 & 0 \\
-\chi u_1 & \chi & 0 & 0 & 0 & 0 & u_1 & 0 & 0 \\
-\psi u_1 & \psi & 0 & 0 & 0 & 0 & 0 & u_1 & 0 \\
0 & 0 & 0 & 0 & 0 & 0 & 0 & 0 & u_1
\end{bmatrix},
$$

$$
A_2 = \begin{bmatrix}
0 & 0 & 1 & 0 & 0 & 0 & 0 & 0 & 0 \\
-u_1 u_2 & u_2 & u_1 & 0 & 0 & 0 & 0 & 0 & 0 \\
K - u_2^2 & -u_1\Gamma & u_2(2 - \Gamma) & -u_3\Gamma & \Gamma & -p\Gamma & -\Gamma & \Gamma & 0 \\
-u_2 u_3 & 0 & u_3 & u_2 & 0 & 0 & 0 & 0 & 0 \\
u_2(K - H) & -u_1 u_2\Gamma & H - u_2^2\Gamma & -u_2 u_3\Gamma & u_2(\Gamma + 1) & -u_2 p\Gamma & -u_2\Gamma & u_2\Gamma & 0 \\
-\varphi u_2 & 0 & \varphi & 0 & 0 & u_2 & 0 & 0 & 0 \\
-\chi u_2 & 0 & \chi & 0 & 0 & 0 & u_2 & 0 & 0 \\
-\psi u_2 & 0 & \psi & 0 & 0 & 0 & 0 & u_2 & 0 \\
0 & 0 & 0 & 0 & 0 & 0 & 0 & 0 & u_2
\end{bmatrix},
$$

$$
A_3 = \begin{bmatrix}
0 & 0 & 0 & 1 & 0 & 0 & 0 & 0 & 0 \\
-u_1 u_3 & u_3 & 0 & u_1 & 0 & 0 & 0 & 0 & 0 \\
-u_2 u_3 & 0 & u_3 & u_2 & 0 & 0 & 0 & 0 & 0 \\
K - u_3^2 & -u_1\Gamma & -u_2\Gamma & u_3(2 - \Gamma) & \Gamma & -p\Gamma & -\Gamma & \Gamma & 0 \\
u_3(K - H) & -u_1 u_3\Gamma & -u_2 u_3\Gamma & H - u_3^2\Gamma & u_3(\Gamma + 1) & -u_3 p\Gamma & -u_3\Gamma & u_3\Gamma & 0 \\
-\varphi u_3 & 0 & 0 & \varphi & 0 & u_3 & 0 & 0 & 0 \\
-\chi u_3 & 0 & 0 & \chi & 0 & 0 & u_3 & 0 & 0 \\
-\psi u_3 & 0 & 0 & \psi & 0 & 0 & 0 & u_3 & 0 \\
0 & 0 & 0 & 0 & 0 & 0 & 0 & 0 & u_3
\end{bmatrix},
$$

With that, the eigenvalues and the corresponding eigenvectors of the matrices are: for matrix A_1,

$$
\Lambda_{A_1} = \text{diag}\big(\lambda_1^{(1)}, \lambda_2^{(1)}, \ldots, \lambda_9^{(1)}\big) = \text{diag}(u_1 - c, \, u_1, \, u_1 + c, \, u_1, \ldots, u_1),
$$

$$
R_{A_1} = \big(r_1^{(1)}, r_2^{(1)}, \ldots, r_9^{(1)}\big) = \begin{bmatrix}
1 & 1 & 1 & 0 & 0 & 0 & 0 & 0 & 0 \\
u_1 - c & u_1 & u_1 + c & 0 & 0 & 0 & 0 & 0 & 0 \\
u_2 & u_2 & u_2 & 1 & 0 & 0 & 0 & 0 & 0 \\
u_3 & u_3 & u_3 & 0 & 1 & 0 & 0 & 0 & 0 \\
H - u_1 c & K/\Gamma & H + u_1 c & u_2 & u_3 & p & 1 & -1 & 0 \\
\varphi & 0 & \varphi & 0 & 0 & 1 & 0 & 0 & 0 \\
\chi & 0 & \chi & 0 & 0 & 0 & 1 & 0 & 0 \\
\psi & 0 & \psi & 0 & 0 & 0 & 0 & 1 & 0 \\
0 & 0 & 0 & 0 & 0 & 0 & 0 & 0 & 1
\end{bmatrix},
$$

for matrix A_2,

$$
\Lambda_{A_2} = \text{diag}\big(\lambda_1^{(2)}, \lambda_2^{(2)}, \ldots, \lambda_9^{(2)}\big) = \text{diag}(u_2 - c, \, u_2, \, u_2 + c, \, u_2, \ldots, u_2),
$$

$$R_{A_2} = \left(r_1^{(2)}, r_2^{(2)}, \ldots, r_9^{(2)}\right) = \begin{bmatrix} 1 & 1 & 1 & 0 & 0 & 0 & 0 & 0 & 0 \\ u_1 & u_1 & u_1 & 1 & 0 & 0 & 0 & 0 & 0 \\ u_2 - c & u_2 & u_2 + c & 0 & 0 & 0 & 0 & 0 & 0 \\ u_3 & u_3 & u_3 & 0 & 1 & 0 & 0 & 0 & 0 \\ H - u_2c & K/\Gamma & H + u_2c & u_1 & u_3 & p & 1 & -1 & 0 \\ \varphi & 0 & \varphi & 0 & 0 & 1 & 0 & 0 & 0 \\ \chi & 0 & \chi & 0 & 0 & 0 & 1 & 0 & 0 \\ \psi & 0 & \psi & 0 & 0 & 0 & 0 & 1 & 0 \\ 0 & 0 & 0 & 0 & 0 & 0 & 0 & 0 & 1 \end{bmatrix},$$

and for matrix A_3,

$$\Lambda_{A_3} = \mathrm{diag}\left(\lambda_1^{(3)}, \lambda_2^{(3)}, \ldots, \lambda_9^{(3)}\right) = \mathrm{diag}(u_3 - c, \ u_3, \ u_3 + c, \ u_3, \ldots, u_3),$$

$$R_{A_3} = \left(r_1^{(3)}, r_2^{(3)}, \ldots, r_9^{(3)}\right) = \begin{bmatrix} 1 & 1 & 1 & 0 & 0 & 0 & 0 & 0 & 0 \\ u_1 & u_1 & u_1 & 1 & 0 & 0 & 0 & 0 & 0 \\ u_2 & u_2 & u_2 & 0 & 1 & 0 & 0 & 0 & 0 \\ u_3 - c & u_3 & u_3 + c & 0 & 0 & 0 & 0 & 0 & 0 \\ H - u_3c & K/\Gamma & H + u_3c & u_1 & u_2 & p & 1 & -1 & 0 \\ \varphi & 0 & \varphi & 0 & 0 & 1 & 0 & 0 & 0 \\ \chi & 0 & \chi & 0 & 0 & 0 & 1 & 0 & 0 \\ \psi & 0 & \psi & 0 & 0 & 0 & 0 & 1 & 0 \\ 0 & 0 & 0 & 0 & 0 & 0 & 0 & 0 & 1 \end{bmatrix};$$

$A_j r_k^{(j)} = \lambda_k^{(j)} r_k^{(j)}$, $j = 1, 2, 3$, and $k = 1, 2, \ldots, 9$.

To find approximate solutions of (23) for multicomponents problem, we use a multidimensional version of the high-resolution wave propagation method described in Section 4. Since the basic idea of the method has been described fully before, and has been implemented in the software packages CLAWPACK (Conservation LAWs PACKage), we will not repeat the whole description here, but refer to the references [19, 23, 25, 45] for the details.

6.1. *Numerical Results in Two Dimensions*

We now show results of some sample two-dimensional multicomponent problems obtained using the high-resolution wave propagation methods with or without local adaptive mesh refinement. To limit the size of this paper, applications of the algorithm to problems in three dimensions will not be disussed here, but is the subject of an ongoing work.

EXAMPLE 6.1.1. We begin by considering a simple interface only problem where the solution consists of a circular copper plate evolving in air with uniform equilibrium pressure $p_0 = 10^5$ Pa and constant particle velocity $(u_1^0, u_2^0) = (10^3 \text{ m/s}, \ 10^3 \text{ m/s})$. In this test, inside a circle of radius $r_0 = 0.16$ m and center $(x_1^0, x_2^0) = (1/4 \text{ m}, 1/4 \text{ m})$, the material is copper modeled by the Cochran–Chan equation of state (6) with the parameter values as given in Table I, while outside the circle, the material is air modeled by the γ-gas law with $\rho_0 = 1.2 \text{ kg/m}^3$ and $\Gamma_0 = 0.4$. Note that this type of interface problem is very fundamental to the development of many multicomponent algorithms in which the aim is to see whether the equilibrium of solution in the pressure, in particular, can be maintained by the method.
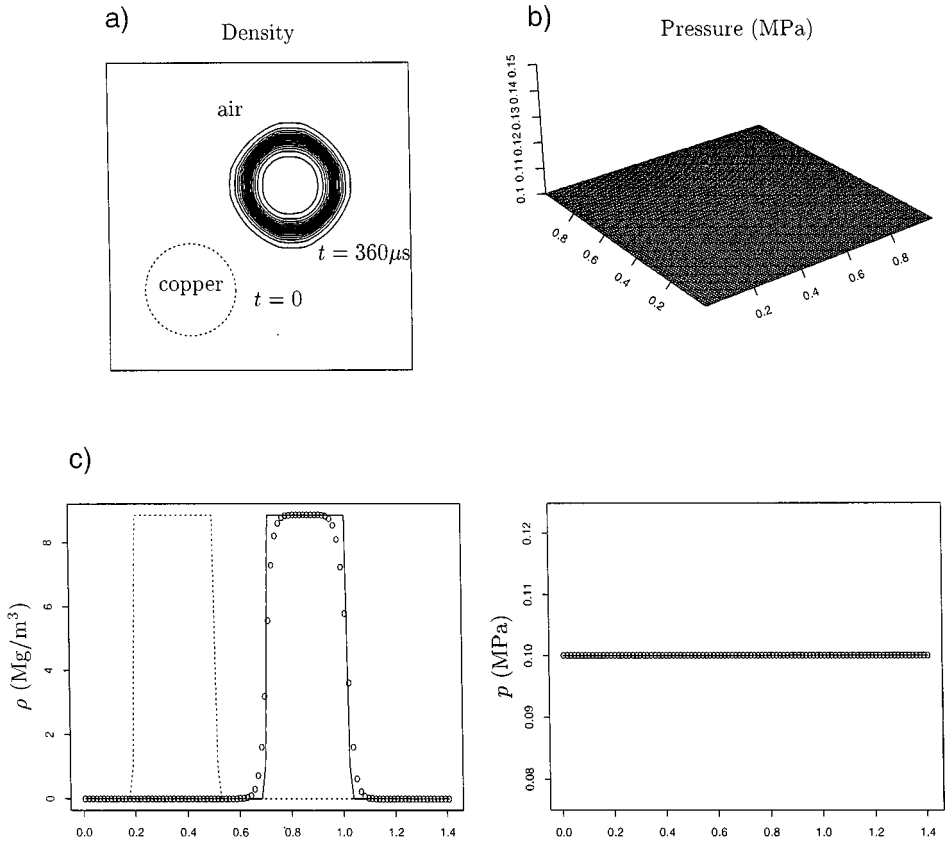
FIG. 7. High-resolution results for the evolution of a circular copper plate in air at time $t = 360\,\mu s$. (a) Contour plot of the density. (b) Surface plot of the pressure. (c) Cross-sectional plots of density and pressure along line $x_1 = x_2$. The solid line in the cross-sectional plot is the exact solution, and the dotted points are the numerical results. The dashed line in the density plots is the initial condition at time $t = 0$. Here the copper is modeled by the Cochran–Chan equation of state (6), while the air is modeled by the standard γ-gas law of ideal gas.

Here we have performed the computations by using (6) to model the numerical mixing between the copper and air. Results obtained using the high-resolution method with the MINMOD limiter, the Courant number $\mu = 0.9$, and a 100×100 uniform grid in a unit square domain, are displayed in Fig. 7, where the 2D contours of the density, 3D surface plot of the pressure, and the cross-section plot of the density and pressure along $x_1 = x_2$ are presented at time $t = 360\,\mu s$. From the displayed profiles, it is easy to observe good agreement of the numerical solutions as compared with the exact results. Notice that the computed pressure remains in the correct equilibrium state p_0 (to be more accurate, the difference of these two is only on the order of machine epsilon), without any unexpected oscillations near the numerically diffused copper–air interface. Moreover, the copper plate retains its circular shape and appears to be very well located.

EXAMPLE 6.1.2.   We are next concerned with a test problem of Miller and Puckett [31] in which a shock wave in molybdenum is interacting with a region of encapsulated MORB liquid. Similar to the initial condition used in Example 5.5, at $x_1 = 0.3$ m, there is a planarly rightward-moving Mach 1.163 shock wave in molybdenum traveling from left to right that is about to collide with a rectangular region $[0.4, 0.7] \times [0, 0.5]\,\mathrm{m}^2$ which contains a MORB
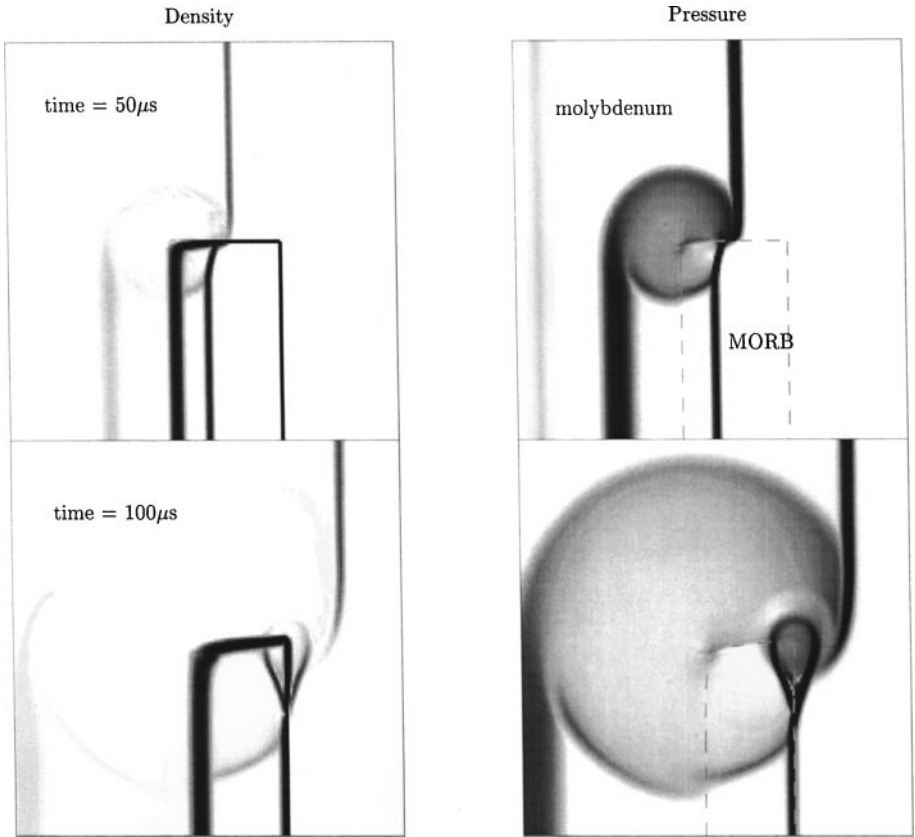
FIG. 8. High-resolution results for a shock wave in molybdenum interacting with an encapsulated MORB liquid. Schlieren-type images for the density and pressure are shown at two different times $t = 50\,\mu s$ and $100\,\mu s$ using a 200×200 grid. The dashed lines appearing in the pressure plot indicate the approximate location of the molybdenum–MORB interface. Both the molybdenum and MORB are modeled by the shock wave equation of state (8).

liquid inside. As before, we use the shock wave equation of state (8) to model the MORB and molybdenum with the material parameters given in Table I.

Figures 8 and 9 show high-resolution results of a sample run using a uniform 200×200 grid on a unit square domain. From Fig. 8, a reasonable resolution of the solution structure (*i.e.*, the diffraction of a shock wave by a MORB liquid) is obtained by using the algorithm where schlieren-type images of the density and pressure are presented at two different times $t = 50\,\mu s$ and $100\,\mu s$; see [31] for a similar test of the problem. The cross section of the results for the same run along line $x_2 = 0.4$ m is drawn in Fig. 9, giving some quantitative information about the density and pressure at the selected times. Note that in that figure we have also included results obtained using the same method but with a finer 400×400 grid, observing good agreement of these two solutions, and free of spurious oscillations in the pressure near the molybdenum-MORB interface.

EXAMPLE 6.1.3. We now consider a generalization the two-component impact problem discussed in Example 5.3 to three components and two dimensions. Here we take the initial condition where in region $x_1 \geq 0.6$ m, we have a leftward going copper plate traveling
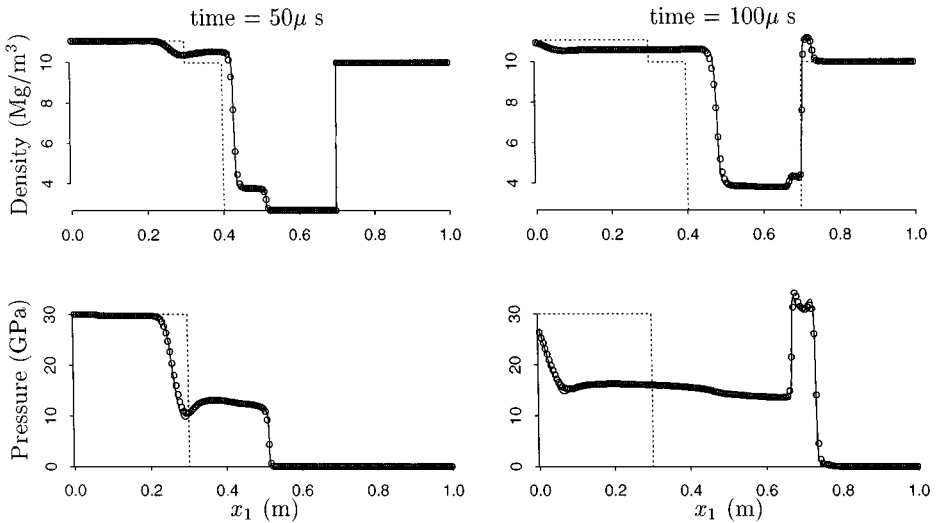
FIG. 9. The cross-sectional plots of the results for the run shown in Fig. 8 along the line $x_2 = 0.4$ m, where the solid lines are results obtained using the same method but with a finer 400×400 grid. The dashed line in each subplot is the initial condition at time $t = 0$.

vertically in a shock tube with speed $u_1 = 1500$ m/s from right to left, while in region $x_1 < 0.6$ m, we have a stationary, horizontal, interface at $x_2 = 0.5$ m that separates a solid inert explosive on the top and a liquid water on the bottom. As in Example 5.3, we assume that all three fluid components are in the usual atmospheric condition initially throughout the domain. We use the Cochran–Chan equation of state (6) to model the copper and explosive, and the Jones–Wilkins–Lee equation of state (5) to model the water. Note that, as before, to deal with the numerical mixing between the copper, explosive, and water, we employ the equation of state of the form (22) for numerical approximation; see Table I again for numerical values to each of the material parameters.

For this problem, we carry out the same runs as done in the previous two examples, and show the numerical results in Figs. 10 and 11. Clearly, because of the impact of the copper plate to the water and explosive, transmitted and reflected shock waves are a result of this action. Note that since the acoustic impedance of explosive is greater than the one for the water, we find a larger shock speed in explosive than the one in water. Moreover, because of the head-on collision betwen the leading edge of the copper plate and the water-explosive interface, generation of a reflected circular wave is observed. It is interesting to mention that this circular wave pattern has already been seen in Fig. 8 where there is a shock wave interacting with a corner of the MORB liquid. The cross-sectional plots of the solutions shown in Fig. 11 give another example of the good agreement of the results as the mesh is refined.

EXAMPLE 6.1.4.   Finally, we are interested in an impact problem that involves the interaction of an underwater aluminum plate to a copper plate. As for the initial condition, on the left half of the unit square domain, the material is copper, while on the right half of the domain, the materials are water on the top and aluminum on the bottom separated by a horizontal interface at $x_2 = 0.4$ m. Here both the copper and water are at rest initially, but there is a leftward-moving speed $u_1 = 1500$ m/s for aluminum that is on the point of hitting
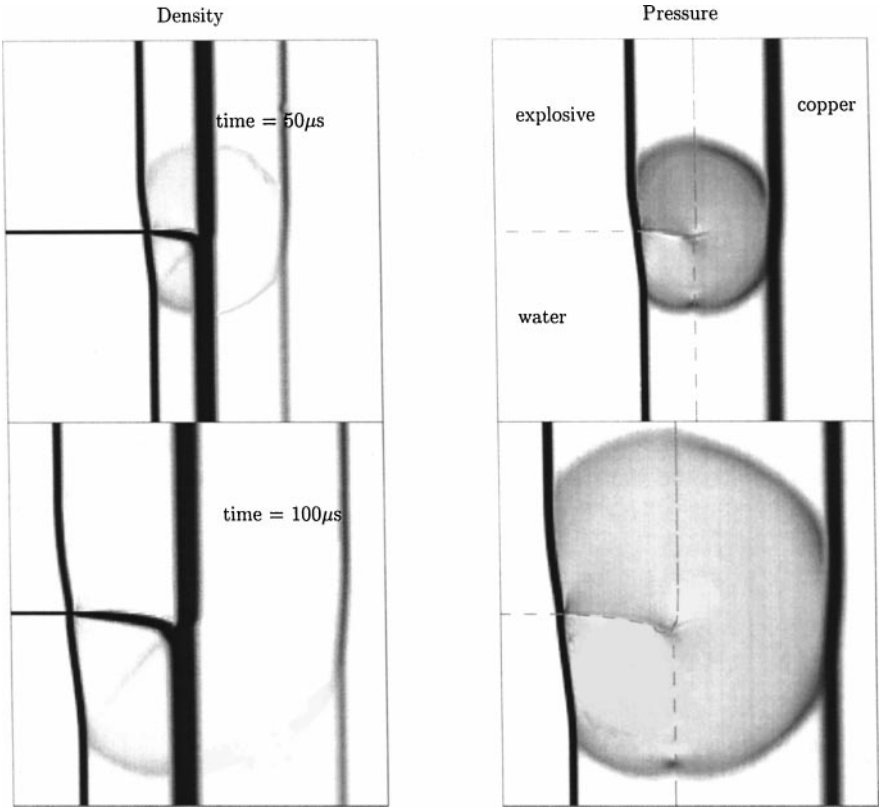
FIG. 10. High-resolution results for a three-component impact problem with a moving copper plate and a stationary interface separating a solid explosive and water. Schlieren-type images for the density and pressure are shown at two different times $t = 50\,\mu s$ and $100\,\mu s$ using a 200×200 grid. The dashed lines appearing in the pressure plot is the approximate location of the copper–explosive–water interface. We model the copper and solid explosive by the Cochran–Chan equation of state (6), and the water by the Jones–Wilkins–Lee equation of state (5).
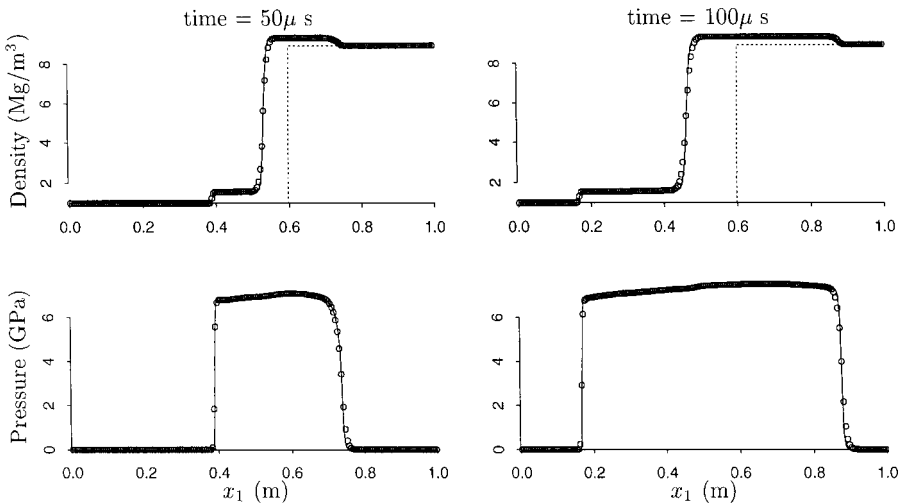
FIG. 11. The cross-sectional plots of the results for the run shown in Fig. 10 along the line $x_2 = 0.4$ m, where the solid lines are results obtained using the same method but with a finer 400×400 grid. The dashed line in each subplot is the initial condition at time $t = 0$.
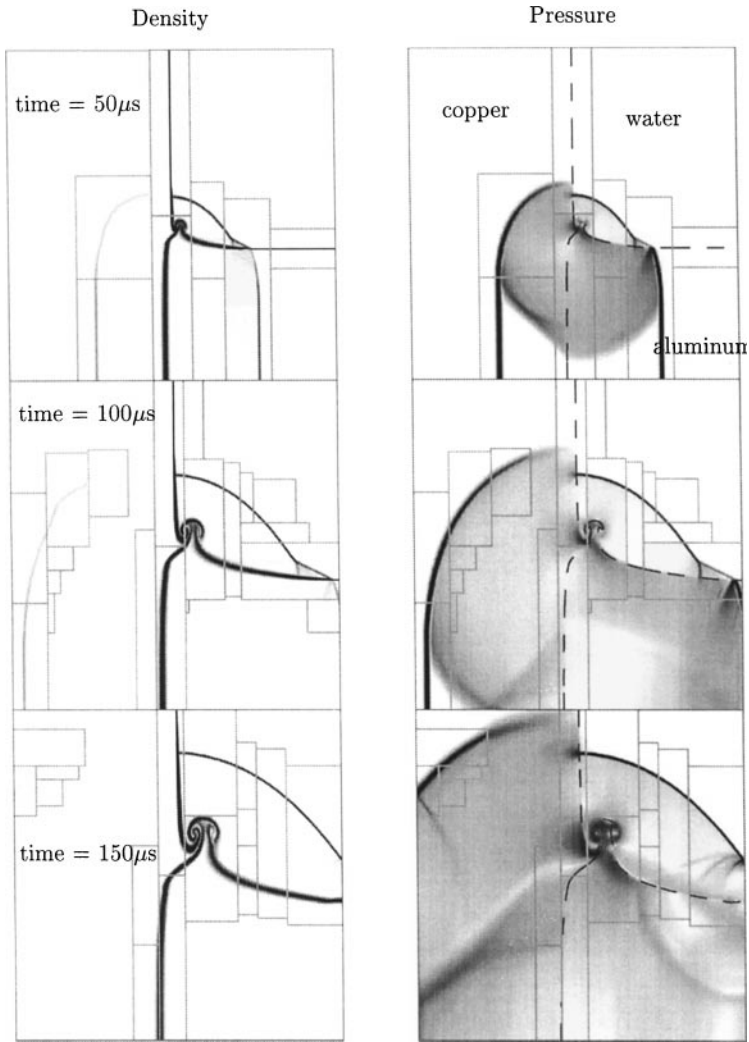
FIG. 12. Local adaptive mesh refinement results for a three-component impact problem with an underwater moving aluminum and a copper. Schlieren-type images for the density and pressure are shown at three different times $t = 50\,\mu s$, $100\,\mu s$, and $150\,\mu s$. Two levels of grid refinement is used with the mesh sizes $h_1 = 1/100$ m on Level 1 and $h_2 = h_1/4$ on Level 2 in both the x_1- and x_2-directions. The dashed lines appearing in the pressure plot is the approximate location of the aluminum–copper–water interface. We model the aluminum, copper, and water by the shock wave equation of state (8).

the copper plate. In addition, we assume that all the materials are in an uncompressed state, and are modeled by the shock wave equation of state (8) with material quantities given in Table I.

In this test, we perform the computation using an adaptive-mesh version of the high resolution scheme; see [3] for more information on how to implement the algorithm for general hyperbolic systems. Note that, in fact, we have modified the software package AMRCLAW of Berger and LeVeque by replacing only the basic integration scheme to our multicomponent algorithm described here, while keeping most of the other routines unchanged. Numerical results with two levels of grid refinement (on Level 1, the mesh size

is $h_1 = 1/100$ m in both the x_1- and x_2-directions, and on Level 2, the mesh is refined by a factor 4) are shown in Fig. 12, where we plot the density and pressure at three different times $t = 50\,\mu s$, $100\,\mu s$, and $150\,\mu s$. From the figure, clearly, because of the impacting of the aluminum to copper, we observe the transmitted and reflected shock waves to the copper and aluminum, respectively. Moreover, on the corner of the copper–water and aluminum–water interfaces, there are a circular shock wave propagating to the water, and a mushroom shape of the interface appearing which separated the copper, aluminum, and water. It should be mentioned that this type of the interface structure is often seen in many geophysical impact problems (cf. [32, 30]). As far as the global picture of the solution is concerned, we have also observed a similar behavior of the solution as the mesh is refined. It is interesting to see that there is a smooth transition of the solutions across the coarse and fine grid interfaces; this means that the basic procedure described in [3] for conservation and wave propagation at grid interface works quite well in this case.

7. CONCLUSIONS

A simple fluid-mixture type algorithm is developed for the numerical resolution of compressible multicomponent problems with real materials modeled by the general Mie–Grüneisen equation of state. The algorithm uses an Eulerian formulation of the equations that are formed by combining a set of effective equations for the material-dependent functions and the Euler's equations of gas dynamics. We use the high-resolution wave propagation method designed originally for single component flow to solve the proposed model system, yielding an easy extension of the method from single-component to multicomponent problems. Numerical results shown in the paper demonstrate the feasibility of the algorithm with the approximate Riemann solver of Roe to a reasonable class of multicomponent problems in both one and two dimensions. In the future, we plan to further extend the algorithm to simulate shock waves in solids with elastic to plastic transition (cf. [34, 52, 55]), and also to simulate shock to detonation transition (cf. [57]). Important physical effects such as cavitation and spallation will be looked into for investigation as well.

REFERENCES

1. R. Abgrall, How to prevent pressure oscillations in multicomponent flow calculations: a quasi conservative approach, *J. Comput. Phys* **125**, 150 (1996).

2. J. B. Bdzil, R. Menikoff, S. F. Son, A. K. Kapila, and D. S. Stewart, Two-phase modeling of deflagration-to-detonation transition in granular materials: A critical examination of modeling issues, *Phys. Fluids* **11**(2), 378 (1999).

3. M. J. Berger and R. J. LeVeque, Adaptive mesh refinement using wave-propagation algorithms for hyperbolic systems, *SIAM J. Numer. Anal.* **35**, 2298 (1998).

4. T. Chang and L. Hsiao, *The Riemann Problem and Interaction of Waves in Gas Dynamics* (Longman, England, 1989).

5. J. F. Clark, S. Karni, J. J. Quirk, P. L. Roe, L. G. Simmonds, and E. F. Toro, Numerical computation of two-dimensional unsteady detonation waves in high energy solids, *J. Comput. Phys.* **106**, 215 (1993).

6. G. Cochran and J. Chan, Shock initiation and detonation models in one and two diemnsions, *UCID-18024* (LLNL, 1979).

7. P. Colella, Glimm's method for gas dynamics, *SIAM J. Sci. Stat. Comput.* **3**(1), 76 (1982).

8. P. Colella and H. M. Glaz, Efficient solution algorithms for the Riemann problem for real gases, *J. Comput. Phys.* **59**, 264 (1985).

9. B. M. Dobratz and P. C. Crawford. Explosive handbook of properties of chemical explosives and explosive simulants, *UCRL-52997* (LLNL, 1985).

10. D. A. Drew and S. L. Passman, *Theory of Multicomponent Fluids* (Springer-Verlag, New York, 1999).

11. B. Einfeldt, C. D. Munz, P. L. Roe, and B. Sjogreen, On Godunov type methods near low densities, *J. Comput. Phys.* **92**, 273 (1991).

12. I. Faille and E. Heintzé, A rough finite volume scheme for modeling two-phase flow in a pipeline, *Comput. Fluids* **28**, 213 (1999).

13. R. P. Fedkiw, T. Aslam, B. Merriman, and S. Osher, A non-oscillatory Eulerian approach to interfaces in multimaterial flows (the ghost fluid method), *J. Comput. Phys.* **152**, 457 (1999).

14. P. Glaister, An approximate linearised Riemann solver for the Euler equations for real gases, *J. Comput. Phys.* **74**, 382 (1988).

15. E. Godlewski and P.-A. Raviart, *Numerical Approximation of Hyperbolic Systems of Conservation Laws*, Applied Mathematical Science 118 (Springer-Verlag, New York, 1996).

16. R. L. Holmes. *A Numerical Investigation of the Richtmyer-Meshkov Instability Using Front Tracking.* Ph.D. thesis (SUNY at Stony Brook, August, 1994), unpublished.

17. R. Jeanloz, Shock wave equation of state and finite strain theory, *J. Geophys. Res.* **94**(B5), 5873 (1989).

18. S. Karni, Hybrid multifluid algorithms, *SIAM J. Sci. Comput.* **17**, 1019 (1996).

19. J. O. Langseth and R. J. LeVeque, A wave propagation method for three-dimensional hyperbolic conservation laws, *J. Comput. Phys.* **165**, 125 (2000).

20. R. J. LeVeque, High resolution finite volume methods on arbitrary grids via wave propagation. *J. Comput. Phys.* **78**, 36 (1988).

21. R. J. LeVeque, *Numerical Methods for Conservation Laws*, 2nd ed. (Birkhäuser-Verlag, Basel, 1992).

22. R. J. LeVeque, Simplified multi-dimensional flux limiter methods, in *Numerical Methods for Fluid Dynamics*, edited by M. J. Baines and K. W. Morton (Oxford Univ. Press, London, 1993), pp. 175–190.

23. R. J. LeVeque, Wave propagation algorithms for multi-dimensional hyperbolic systems, *J. Comput. Phys.* **131**, 327 (1997).

24. R. J. LeVeque and K.-M. Shyue, One-dimensional front tracking based on high resolution wave propagation methods, *SIAM J. Sci. Comput.* **16**, 348 (1995).

25. R. L. LeVeque. CLAWPACK. 2000. Available from netlib.att.com in netlib/pdes/claw or on the Web at the URL http://www.amath.washington.edu/rjl/clawpack.html.

26. C. L. Mader, *Numerical Modeling of Detonations* (Univ. of Californa Press, Berkeley, 1979).

27. S. P. Marsh, *LASL Shock Hugoniot Data* (Univ. of California Press, Berkeley, 1980).

28. R. G. McQueen, S. P. Marsh, J. W. Taylor, J. N. Fritz, and W. J. Carter. The equation of state of solids from shock wave studies. In *High Velocity Impact Phenomena*, edited by R. Kinslow (Academic Press, San Diego, 1970), pp. 293–417.

29. R. Menikoff and B. Plohr, The Riemann problem for fluid flow of real materials, *Rev. Mod. Phys.* **61**, 75 (1989).

30. G. H. Miller, Jetting in oblique, asymmetric impacts, *ICARUS* **134**, 163 (1998).

31. G. H. Miller and E. G. Puckett, A high order Godunov method for multiple condensed phases, *J. Comput. Phys.* **128**, 134 (1996).

32. G. H. Miller and E. G. Puckett, Numerical simulation of jetting impacts. in Proceedings of the 20th Intl. Symp. *on Shock Waves* (World Scientific, Singapore, 1996). Vol. 2, pp. 1467–1472.

33. L. Mottura, L. Vigevano, and M. Zaccanti, An evaluation of Roe's scheme generalization for equilibrium real gas flows, *J. Comput. Phys.* **138**, 354 (1997).

34. K. Nagayama, Solution of the high-pressure Riemann problem for solids including rigidity effects, *J. Phys. Soc. Japan* **58**, 1631 (1989).

35. K. Nagayama and T. Murakami, Numerical analysis of converging shock waves in concentric solid layer, *J. Phys. Soc. Japan* **40**, 1479 (1976).

36. W. J. Rider, An adaptive Riemann solver using a two-shock approximation, *Comput. Fluids* **28**, 741 (1999).

37. P. L. Roe, Fluctuations and signals—A framework for numerical evolution problems. in *Numerical Methods for Fluid Dynamics*, edited by K. W. Morton and M. J. Baines (Academic Press, San Diego, 1982), pp. 219–257.

38. P. L. Roe. Upwind schemes using various formulations of the Euler equations, in *Numerical Methods for the Euler Equations of Fluid Dynamics*, edited by F. Angrand, A. Dervieux, J. A. Desideri, and R. Glowinski (Soc. for Industr. & Appl. Math., 1985).

39. J. E. Romate, An approximate Riemann solver for a two-phase flow model with numerically given slip relation, *Comput. Fluids* **27**, 455 (1998).

40. A. L. Ruoff, Linear shock-velocity-particle-velocity relationship, *J. Appl. Phys.* **38**(13), 4976 (1967).

41. R. Saurel and R. Abgrall, A multiphase Godunov method for compressible multifluid and multiphase flows, *J. Comput. Phys.* **150**, 425 (1999).

42. R. Saurel and R. Abgrall, A simple method for compressible multifluid flows, *SIAM J. Sci. Comput.* **21**, 1115 (1999).

43. R. Saurel, M. Larini, and J. C. Loraud, Exact and approximate Riemann solvers for real gases, *J. Comput. Phys.* **112**, 126 (1994).

44. K.-M. Shyue, An efficient shock-capturing algorithm for compressible multicomponent problems, *J. Comput. Phys.* **142**, 208 (1998).

45. K.-M. Shyue, A fluid-mixture type algorithm for compressible multicomponent flow with van der Waals equation of state, *J. Comput. Phys.* **156**, 43 (1999).

46. K.-M. Shyue, A volume-of-fluid type algorithm for compressible two-phase flows, in *Hyperbolic Problems: Theory, Numerics, Applications*, Intl. Series of Numerical Mathematics (Birkhäuser-Verlag, 1999). Vol. 130.

47. R. W. Smith, AUSM (ALE): a geometrically conservative arbitrary Lagrangian-Eulerian flux splitting scheme, *J. Comput. Phys.* **150**, 268 (1999).

48. J. Smoller, *Shock Waves and Reaction-Diffusion Equations* (Springer-Verlag, New York, 1982).

49. H. B. Stewart and B. Wendroff, Two-phase flows: models and methods, *J. Comput. Phys.* **56**, 363 (1984).

50. P. K. Sweby, High resolution schemes using flux limiters for hyperbolic conservation laws, *SIAM J. Numer Anal.* **21**, 995 (1984).

51. I. Toumi, A. Kumbaro, and H. Paillere. Approximate Riemann solvers and flux vector splitting schemes for two-phase flow, in *Von Karman Institute for Fluid Dynamics*, Lecture Series on Computational Fluid Dynamics 1999-03 (Von Karman Institute, Belgium, 1999).

52. M. B. Tyndall, Numerical modelling of shocks in solids with elastic-plastic conditions, *Shock Waves* **3**, 55 (1993).

53. G. B. Wallis, *One-Dimensional Two-Phase Flow* (McGraw-Hill, New York, 1969).

54. A. B. Wardlaw, Jr. and H. U. Mair, Spherical solutions of an underwater explosion bubble, *Shock Vib.* **5**, 89 (1998).

55. M. L. Wilkins, *Computer Simulation of Dynamic Phenomena* (Springer-Verlag, New York, 1999).

56. Y. B. Zel'dovich and Y. P. Raizer, *Physics of Shock Waves and High-Temperature Hydrodynamic Phenomena* (Academic Press, San Diego, 1967), Vol. II.

57. J. Zhang, Z. Duan, and J. Ding, Simulating shock to detonation transition: algorithm and results, *J. Comput. Phys.* **150**, 128 (1999).